Thermal architecture of cratonic India and implications for decratonization of the Western Dharwar Craton: Evidence from mantle xenoliths in the Deccan Traps

Article *in* Lithos · February 2021

DOI: 10.1016/j.lithos.2020.105927

CITATIONS
12

READS
624

3 authors, including:

A. G. Dessai
34 PUBLICATIONS **493** CITATIONS
SEE PROFILE

Anthony Viegas
Goa University
7 PUBLICATIONS **87** CITATIONS
SEE PROFILE

Contents lists available at ScienceDirect

LITHOS

journal homepage: http://ees.elsevier.com

Research Article

Thermal architecture of cratonic India and implications for decratonization of the Western Dharwar Craton: Evidence from mantle xenoliths in the Deccan Traps

A.G. Dessai [a,b,*], A. Viegas [b], W.L. Griffin [c]

[a] A/4, Primrose Apartments, Baner, Pune 411045, India
[b] School of Earth Ocean and Atmospheric Sciences, Goa University, Taleigao Plateau, Goa 403 206, India
[c] ARC Centre of Excellence for Core to Crust Fluid Systems and GEMOC ARC National Key Centre, Earth and Planetary Sciences, Faculty of Science and Engineering, Macquarie University, NSW 2109, Australia

ARTICLE INFO

Article history:
Received 12 July 2020
Received in revised form 22 November 2020
Accepted 4 December 2020
Available online xxx

Keywords
Mantle lherzolite
Granulite xenoliths
Lower crust
Thermal structure
Decratonization
Dharwar Craton
Indian shield

ABSTRACT

The mantle beneath the Western Dharwar Craton of the Indian shield comprises a suite of refractory and fertile peridotites and mafic granulites. Detailed petrographic studies coupled with new mineral analysis and geothermobarometric estimations permit to decipher the thermal architecture and get an insight into the evolution of this ancient craton. The refractory rocks are coarse grained harzburgites/dunites, whereas the more fertile ones are at times, porphyroclastic lherzolites. Both show a similar range of equilibration temperatures and pressures indicating intermixing between the two at various levels. The peridotites contain undeformed interstitial REE-enriched clinopyroxene, phlogopite, apatite and carbonates recording post-kinematic modal and cryptic metasomatic events in the Precambrian cratonic lithosphere. Xenoliths of mafic granulite contain layers of clinopyroxenite which also vein the granulite. The P-T range of the granulites overlaps that of the ultramafic rocks.This study in combination with previous investigations reveals a distinct change in the thermal architecture of the craton from a warm/hot geotherm in the Proterozoic to a highly perturbed, still hotter geotherm of the Palaeocene. The Cenozoic thermotectonic rifting episodes heated, refertilized and thinned the bulk of the cratonic lithosphere beneath the Western Dharwar Craton, which has witnessed the most re-activation among cratons of the Indian shield. The waning of the Deccan Traps volcanism in Palaeocene time saw the reworking of ancient cratonic lithosphere and its replacement by non-cratonic, juvenile mantle and magmatic accretions, indicated by compound xenoliths. Differing petrological and geochemical characteristics of refractory xenoliths and fertile lherzolites serve to constrain the relative timing and composition of non-cratonic lithosphere. By the end of the Palaeocene the Western Dharwar Craton was characterised by a thermal high, an attenuated continental lithosphere (60–80 km), and a thin crust (<10- ~ 21 km), reflecting the decratonization of at least the western part of the Western Dharwar Craton.

1. Introduction

Cratons consist of thick lithospheric domains which have remained stable for long geologic periods (>1 Ga) since their inception in the Archaean (Pearson et al., 1995). They are characterised by cold cratonic geotherms (Boyd et al., 1985; Chevrot and Zao, 2007; Evans et al., 2011; Jaupart and Mareschal, 1999). While some cratons have thick mantle keels (Shapiro et al., 1999; Sodoudi et al., 2013) which have survived reworking from plate tectonics, others were partially modified in more recent times (Eggler and Furlong, 1991; Menzies et al., 1993, 2007; Zheng et al., 2004, 2006; Liang et al., 2013; Aulbach et al., 2017a).

The Western Dharwar Craton (WDC), one of the oldest in the Indian shield, has long been known to be different from other cratons of comparable age. Some workers are of the opinion that the Indian shield in general has a thin lithosphere (Polet and Anderson, 1995; Rychert and Shearer, 2009) which has been subjected to Phanerozoic thermomagmatic reworking (Dessai et al., 1999, 2004; Griffin et al., 2009; Kiselev et al., 2008; Kumar et al., 2007b). Most workers carry the contrary view, that the WDC has a thick lithospheric keel that is least affected by Phanerozoic tectonothermal events/perturbations (Leelanandam et al., 2006; Ramesh et al., 2010; Ravi Kumar and Mohan, 2005) among the ensemble of cratons of the Indian shield.

Most deductions so far on the deep lithospheric structure of the WDC have been based primarily on remotely sensed data, locally supported by xenocrysts (Griffin et al., 2009) and xenoliths in kimberlites (Ganguly and Battacharya, 1987; Nehru and Reddy, 1989; Pattanaik et al., 2020) from the neighbouring Eastern Dharwar cra-

* Corresponding author at: A/4, Primrose Apartments, Baner, Pune 411045, India.
E-mail address: ashokadessai@gmail.com (A.G. Dessai)

https://doi.org/10.1016/j.lithos.2020.105927
0024-4937/

ton (EDC). A rare suite of spinel lherzolite and mafic granulite xenoliths from the western Deccan Traps (DT) at Murud-Janjira illustrates the petrological and geochemical composition of the lithospheric mantle beneath this poorly sampled region of the WDC. The prime objective of this study is to understand the Phanerozoic evolution of the WDC based on new petrographic and compositional data combined with that from the literature. We assess the palaeo-thermal structure of the subcontinental lithospheric mantle (SCLM) and its subsequent modification on the basis of different suites of xenoliths (present study and those reported earlier) during the course of India's journey from east Gondwana to its present location. This enables us to address the fundamental question on the present nature of the cratonic keel beneath the WDC. We propose that the Archaean keel beneath the WDC was thinner than other cratons and was subjected to reworking beginning in the Proterozoic and continuing through the Phanerozoic, finally resulting in decratonisation of the WDC.

2. Geotectonic Framework

The Indian shield (Fig. 1) is an agglomeration of several cratons (Naqvi and Rogers, 1987) that broadly evolved during Precambrian and is bounded variously by mobile belts, rift zones, thrusts and/or granitic batholiths. The shield is divided into two blocks by a major ENE-WSW trending tectonic belt referred to in modern literature as the Central Indian Tectonic Zone (CITZ) (Radhakrishna and Ramakrishnan, 1988), and which corresponds to the satellite imagery feature known as the Narmada-Son lineament. The latter represents a major tectonic zone also known as the SONATA (Son-Narmada-Tapti) rift system that marks the eastern arm of the Cambay triple junction (Burke and Dewey, 1973). It separates the Bundelkhand and Aravalli cratons in the north from the Dharwar craton in the south. The latter itself consists of two cratonic blocks, the Mesoarchaean WDC and the Neoarchean EDC (Bhaskar Rao et al., 2008; Nutman et al., 1992) which are sutured along the Chitradurga Shear Zone and the Closepet Granite batholith. Both cratonic blocks are brought in contact with the Southern Granulite Terrain (SGT) in the south along the E-W Palghat-Cauvery shear belts (Naqvi and Rogers, 1987).

Several types of investigations have been undertaken to decipher the deep structure of the Dharwar craton (Chadwick et al., 2000; Chardon et al., 2008; Gokarn, 2003; Kaila et al., 1979; Vijaya Rao et al., 2015a, 2015b). However, these studies have been unable to provide a definitive picture, since the composition and thermal characteristics of the deep rocks in particular were not adequately known.

The WDC comprises a granite-greenstone terrain which consists of a basement of TTG gneisses (Peninsular Gneissic Complex, 3.3–3.0 Ga) that contain tectonically transported enclaves of older supracrustals assigned to the Sargur Group with komatiitic ultramafites dated to 3.352 ± 110 Ga (Sm/Nd wholerock isochron; Jayananda et al., 2008). These are widely overlain by supracrustal rocks (late Archaean-early Proterozoic) deposited in ensialic, intra-cratonic rift basins (Chadwick et al., 1992) and which are assigned to the Dharwar Supergroup (Swami Nath and Ramakrishnan, 1981). The associated diapiric plutons of potassic granites are dated to 2.614 ± 10 Ga (SIMS U—Pb zircon ages) (Jayananda et al., 2006) indicative of the reworking of the craton. Proterozoic mafic dyke swarms (2.367 ± 1Ga; Hall et al., 2007) intrude the supracrustals. A large part of the northern portion of the craton is covered by the lavas of the Deccan Traps (64–67 Ma; Hofmann et al., 2000). The regional foliation within the craton trends NW-SE in the north and turns to N-S towards the south. This cratonic block stabilized around 3.3–3.0 Ga and, is delimited in the north by the CITZ, and in the west by the western margin rift represented by the Arabian Sea. In the east, the craton is bounded jointly by the NW-SE trending Chitradurga shear zone (Kaila et al., 1979) and

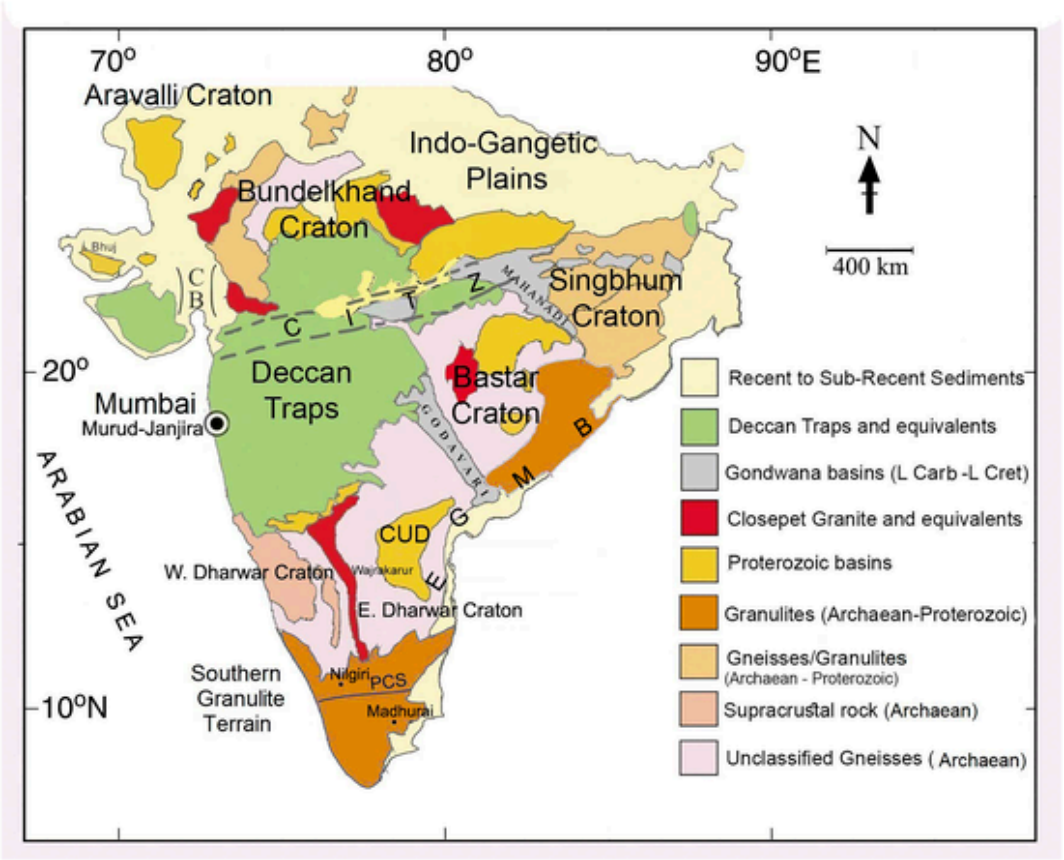

Fig. 1. Generalised geotectonic framework of the Indian shield depicting the configuration of Archaean cratons, the Deccan Traps province, and the xenolith locality Murud-Janjira, CITZ: Central Indian Tectonic Zone, CB: Cambay basin, CUD: Cuddapah basin, EGMB: Eastern Ghat Mobile Belt (modified from Geological Survey of India, 1993).

N-S Closepet Granite (~2.51 Ga; Friend and Nutman, 1992), the batholithic complex through which it is sutured with the EDC. There is yet another view (Chadwick et al., 2000) that the EDC is thrust over the WDC along the oblique shear, which was later penetrated by the Kalyandurg kimberlites during the Proterozoic (Griffin et al., 2009). The EDC consists of a remobilised gneissic basement which comprises granodioritic gneisses and has a high proportion of granitoids that vary in age from about 2.7–2.5 Ga with subordinate supracrustals of an oceanic intra-arc affinity (Krogstad et al., 1991).

The northern portion of the WDC, particularly the terrain immediately to the south of the CITZ, which is largely covered by DT, has been investigated by geophysical techniques including gravity, seismic refraction and reflection profiling, electrical and magnetotelluric (MT) studies, and geothermal logging (Mahadevan, 1994 and references therein). The terrain to the south of the DT has been investigated by the (E-W) Kavali-Udupi and (N-S) Kupam-Palani DSS, and the Chikmagalur-Perur DSS reflection profile and MT profile (Kaila et al., 1979; Reddy et al., 2003; Mandal et al., 2018; Gokarn, 2003; Abdul Azeez et al., 2015 resp.) An anomalously high lithosphere thickness is suggested from receiver function (RF) studies (Oreshin et al., 2011). The western and the northern margins of the craton show positive Bouguer anomalies (+70 mGals) (Glennie, 1951; Takin, 1966) and a negative magnetic anomaly at Mumbai. This implied thinning is supported by DSS profiles that suggest shallowing of the Moho (Kaila, 1988) from about 31 km near the coast at Mahad (south of Mumbai), to about 18–21 km at Bilimora (north of Mumbai), where the upper crust is estimated to be only 6–8 km thick (Kaila et al., 1981).

A thin lithosphere beneath the craton (<100 km) was proposed by Negi et al. (1987), and Kumar et al., (2007) among others, whereas Gupta et al. (2003), Maurya et al. (2016) and others suggest a thicker lithosphere (>160 km) which thins towards the west to 70 km at Valsad (Singh et al., 2014). The oceanic region in the west extending approximately from 25° N to 10° S is characterised by the Laxmi and Laccadive-Chagos ridges which are relict fragments of continental lithosphere with no oceanic crust over the topographic features, consistent with the absence of magnetic stripes. The Arabian Sea, in particular, from the east coast of Africa to the west coast of India, is characterised by low shear wave velocities (Nataf et al., 1984). Furthermore, the analogue of the west coast dyke-swarm (Dessai and Viegas, 1995) has been identified on the Mahe and North Islands of the Seychelles (Devey and Stephens, 1991, 1992). This is ascribed to the opening of the Arabian Sea which involved attenuation, extension, thinning and foundering of continental crust from the subjacent mantle along a system of extensional faults (Dessai and Bertrand, 1995) which locally may have a listric configuration as has been observed in several parts of the world (Geoffroy et al., 1998; Nielsen and Brooks, 1981).

3. Petrology of XXenoliths

Profuse late alkaline dyke swarms (Dessai and Bertrand, 1995; Dessai and Viegas, 1995) were intruded parallel to the western and northern margins of the craton towards the close of the Deccan magmatism. Tephriphonolites, melanephelinites, carbonatites and lamprophyres, the youngest of the late intrusive members of the swarm (Dessai and Viegas, 1995), host a wide range of igneous xenoliths and megacrysts, along with a variety of upper and lower crustal xenoliths of granitic gneisses, granites, schistose metasediments and granulites (Dessai et al., 1990) that show varying changes due to anatexis. The lower crustal and mantle xenoliths from among these are the most significant to elucidate the composition, thermal structure and the overall evolutionary history of the lithospheric column of the WDC. Mantle xenoliths are also found in nephelinite-basanite plugs in Bhuj (Kutch region of Gujarat) (Dessai et al., 1999; Karmalkar et al., 2000, 2005; Mukherjee and Biswas, 1988).

The xenoliths from Murud-Janjira are largely free from the fracturing associated with rapid decompression seen in kimberlite xenoliths and few have undergone slight alteration by way of serpentinisation of olivine along grain boundaries and fractures. Original microstructures are clearly observable (Fig. 2). The xenoliths have been categorized into (i) ultramafic, (ii) mafic and (iii) felsic groups (Dessai et al., 1999, 2004; Dessai and Vaselli, 1999). They vary in size from 0.5 mm to 3 cm; the felsic ones are generally larger reaching up to 5 cm. In this paper we describe a suite of spinel lherzolite-harzburgite/dunite and mafic granulite xenoliths.

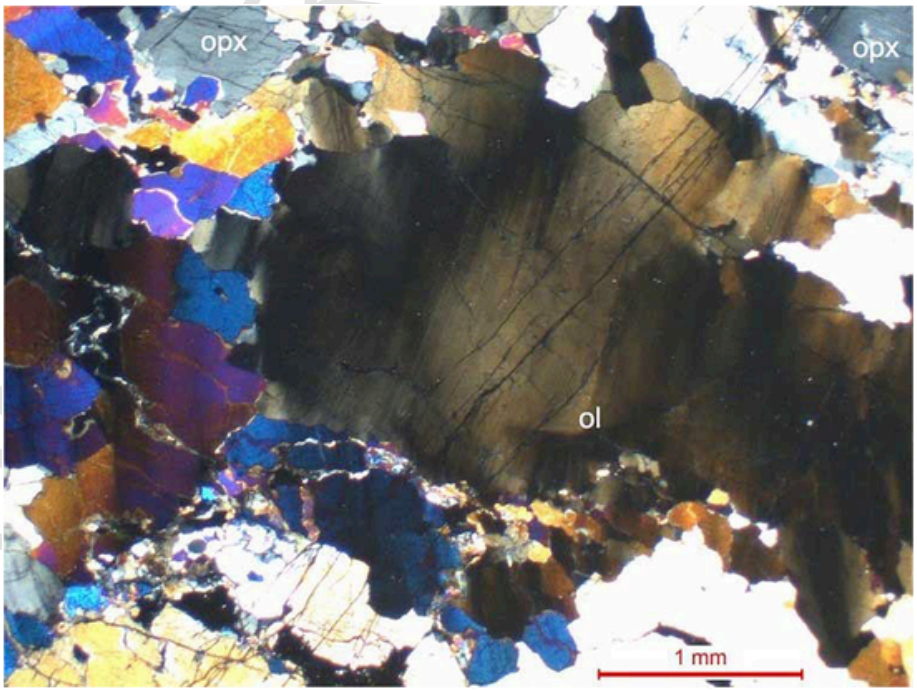

Fig. 2. Olivine porphyroclasts with deformation lamellae, undulose extinction and development of subgrain neoblasts along grain boundaries (ol: olivine, opx: orthopyroxene) (BxP).

3.1. Spinel Peridotites

The ultramafic group ($n = 42$) can be classified on textural considerations into two subtypes following Mercier and Nicolas (1975), Boyd and Nixon (1975) and Nixon et al. (1981) as (i) coarse granular with refractory compositions and (ii) finer grained, originally protogranular grading into porphyroclastic, sheared mylonitic fabric and mosaic equigranular. Clinopyroxenites and websterites with or without garnet and subordinate wehrlites have been described by Dessai et al. (2004).

We report here the occurrence of harzburgite/dunite and spinel lherzolite and mafic granulite xenoliths (coordinates of xenolith localities are in Table 2) in the western Deccan Traps from Murud-Janjira and Borlai-Korlai (10 km north of Murud-Janjira). They belong to the Cr-diopside peridotite group of Wilshire and Shervais (1975) equivalent to the Type I peridotite xenoliths of Frey and Prinz (1978). Modally they consist primarily of olivine, orthopyroxene, clinopyroxene and spinel/Ti-magnetite, with minor amounts of amphibole, carbonates, sulfides and glass. The presence of amphibole, micas and carbonates suggest that the lherzolites have been subjected to modal metasomatism. Texturally they are coarse equigranular (protogranular) to porphyroclastic, and the grain size varies from 0.5–4.0 mm. In places, they are foliated with tabular olivine and spinel. Olivine porphyroclasts display kink bands, deformation lamellae, undulose extinction and development of subgrain neoblasts along grain boundaries (Fig. 2). The harzburgites and dunites are texturally akin to the spinel lherzolites although they differ in modal composition.

Foliated lherzolites locally show tabular olivines with 120° triple point junctions (Fig. 3). Orthopyroxene occurs as slightly elongate grains that exhibit stretching and deformation; they sometimes display deformation lamellae and kink bands and may contain inclusions of olivine. Clinopyroxene is generally irregular, interstitial and largely free from deformation. It is at times spatially associated with phlogopite and spinel. Spinel-pyroxene symplectites, as break-down products of garnet are quite common. Rare clinopyroxene veins traverse the peridotites.

A summary of the textural and compositional characteristics of xenoliths is presented in Table 1. They are largely xenomorphic granular; rarely clinopyroxene exhibits a weak planar fabric defined by preferentially oriented clinopyroxene and spinel.

3.2. Mafic Granulites

The mafic xenoliths (this study: Krl/148, Krl/150, Krl/152, Krl/160, Krl/168, Krl/170: 18°.5363 N, 72°.9081 E) comprise two-pyroxene granulites with or without garnet. Most xenoliths display compositional layering on a scale of mm to cm defined by mafic-rich layers of pyroxene plus garnet and plagioclase-rich bands, representing metamorphic banding. A few exhibit foliation defined by mafic minerals and plagioclase. The textures in general range from coarse granular to porphyroclastic to granuloblastic. The dominant texture is polygonal granoblastic, suggesting annealing in a static environment. Clinopyroxene, orthopyroxene, plagioclase and garnet are the main mineral phases with accessory proportions of phlogopite, apatite, rutile and opaques. Clinopyroxene compositions (Fig. 4) are aluminous ferroan diopside (Morimoto et al., 1988), with generally higher Al^{vi}/Al^{iv} and lower Ti/Al ratios than those in clinopyroxenites and websterites, which is characteristic of high-pressure environments (Dessai et al., 1999, 2004).

Most garnets from the xenolith suite are rich in pyrope. Many show similarities to those from eclogites in kimberlites and in gneisses (e.g. Coleman et al., 1965). Many samples exhibit layering of mafic and felsic domains on a millimeter scale wherein individual layers display granular microtextures. Compound xenoliths are less abundant with interlayering of mafic granulite and clinopyroxenite/websterite. At places clinopyroxenite cross-cuts the granulite layering. The latter is granoblastic whereas the clinopyroxenite exhibits cumulate textures. The cumulate rocks are interpreted as magmatic accretions at the crust-mantle boundary (Dessai et al., 2004).

1. Analytical Technique and P-T Computations

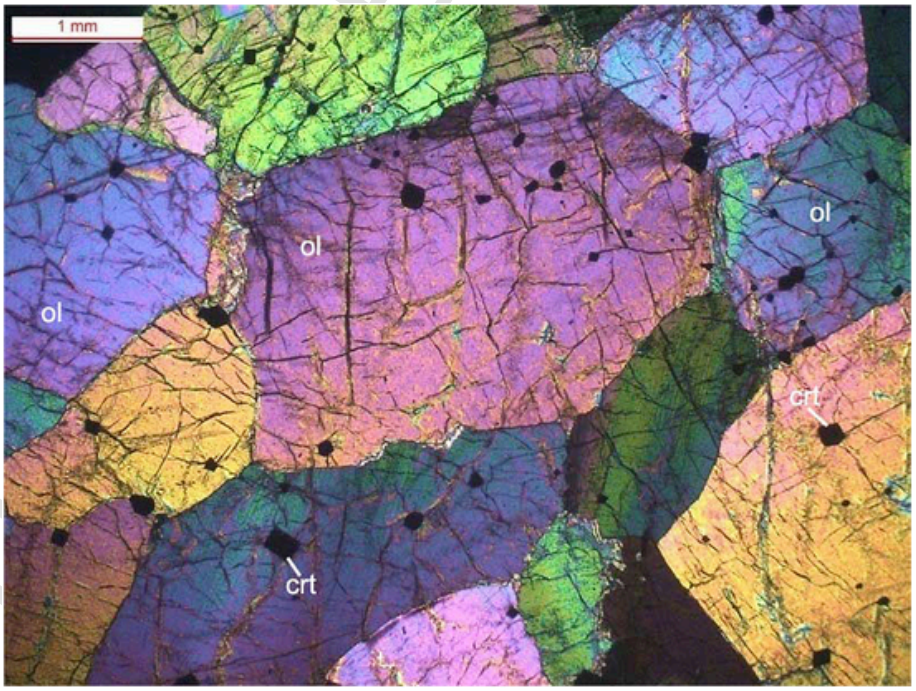

Fig. 3. Foliated lherzolites show tabular olivines with 120° triple point junctions and sub-idiomorphic chrome spinels (ol: olivine, crt: chromite) (BxP).

Table. 1
Summary of Petrological Characteristics of Xenoliths (this study inclusive) in dykes from WDC [1].

Xenolith Type/ Group	Felsic Granulite	Mafic Granulite	Pyroxenite	Pyroxenite	Peridotite
Size	2–15.0 cm	2- > 10.0 cm	0.5–2.0 cm	0.3–2.0 cm	0.4–3.0 cm
Protolith	Leucogabbro	Melagabbro	Clinopyroxenite	Websterite	Spinel lherzolite/Harzburgite-Dunite
Texture	Mosaic granular	Metaigneous/ Layered	Cumulitic/ Metaigneous	Hypidiomorphic granular	Allotriomorphic granular/Porphyroclastic-Protogranular
Modal Composition (vol%)					
Ol	–	–	–	tr	85–62/76–92
Cpx	1–41	2–67	90	>80	05–20/6 = 20
Opx	tr	tr-36	tr-10	tr-15	08–15/1–2
Spnl/Ti-mag.	–	–	–	–	0.5–3.0/0.5–1.0
Plg.	58–98	2–54	tr	–	–
Gnt	tr	tr-33	tr	–	–
Phlg	tr	tr	tr-10	tr-05	–
Others	rtl + amp + apt + sld.	rtl + apt + sld.	apt + sld.	ol + apt + sld.	amp + cbn
Mineral chemistry (mole %)					
Ol.	–	–	–	–	$Fo_{90->91.5}$
Opx.	$Ca_{0.36}$	Ca_{1}	$Ca_{0.8–1.4}$	$Ca_{1.4–1.5}$	$Ca_{0.7–2.0}$
	Mg_{46-64}	$Mg_{65–83}$	$Mg_{77–83}$	$Mg_{72–88}$	$Mg_{89–90}$
	Fe_{53-35}	$Fe_{33–15}$	$Fe_{22–15}$	$Fe_{26–10}$	$Fe_{8.0–8.6}$
	Mg # 0.68	Mg # 0.82–0.92	Mg # 0.83–0.85	Mg # 0.753–0.91	Mg # 0.90–0.94
Cpx.	Ca_{50-42}	Ca_{46}	Ca_{45-47}	Ca_{45-48}	$Ca_{48–49}$
	Mg_{33-38}	Mg_{39-46}	Mg_{46-42}	Mg_{49-40}	Mg_{47-48}
	Fe_{17-20}	Fe_{14-7}	Fe_{12-7}	Fe_{6-12}	Fe_{2-3}
	Mg # 0.68	Mg# 0.82–0.92	Mg # 0.83–0.92	Mg # 0.85–0.99	Mg # 0.93–0.94
Gnt.	Ca_{20-15}	Ca_{12-15}	Ca_{19-20}	Ca_{11}	–
	Mg_{30-39}	Mg_{45-52}	Mg_{23-30}	Mg_{50-72}	–
	Fe_{50-46}	Fe_{38-33}	Fe_{48-53}	Fe_{35-16}	–
Plg. I	Ca_{30-35}	Ca_{46-68}	–	–	–
	Na_{69-63}	Na_{52-31}	–	–	–
	$K_{0.4–2.0}$	K_{2-1}	–	–	–
Plg. II	–	Ca_{30-36}	–	–	–
	–	Na_{68-64}	–	–	–
	–	K_{2-0}	–	–	–
Plg. III	–	Ca_{75}	–	–	–
	–	Na_{24}	–	–	–
	–	$K_{0.5}$	–	–	–
Ti-mag./Spnl.	–	–	TiO_2 wt% 11.59–13.01	–	Al_2O_3 wt% 32–53
	–	–	FeO wt% 81.81–83.55	–	Cr_2O_3 wt% 16–37
	–	–	–	–	Mg # 0.66–0.77

ol: olivine, opx: orthopyroxene, cpx: clinopyroxene, gnt: garnet, plg: plagioclase, phlg: phlogopite, amp: amphibole, cbn: carbonate, apt: apatite, spd: sulphide, Ti-mag./spnl: /Ti-magnetite/spinel, rtl: rutile, Fo: forsterite, tr: trace, Mg#: Mg/(Mg + Fe). ([1] after Dessai and Vaselli, 1999; Dessai et al., 1999; 2003 and this study).

Minerals (n:17 of 42) were analysed using a JEOL 6400R microprobe analyzer under standard operating conditions at the Centre for Microscopy and Microanalysis, The University of Western Australia. Accelerating potential of 15 kV and a specimen current of 10 nA were used. Between 5 and 24 analyses were made on each phase in each rock, and up to 9 analyses in some core-rim traverses. A range of natural and synthetic standards was used for standardization. The instrument and analytical details are described elsewhere (Dessai et al., 1990). The mineral analyses were provided by the late N. M. S. Rock. The EPMA analyses (average of a minimum of four point analyses) of mineral phases from the xenoliths are presented in Table 2.

Equilibration temperatures of xenoliths were estimated using two-pyroxene thermometers (Fe—Mg exchange between opx and cpx) of Wells (1977), Wood and Banno (1973), Brey and Kohler (1990) and Putirka (2008). Recognising the limitations of geobarometers applicable to spinel peridotite-facies rocks, the equilibration of co-existing pyroxenes [barometer originally proposed by Mercier et al., 1984 and updated by Putirka, 2008] was employed to calculate equilibration pressures. Different methods of P-T calculation yield divergent results that may arise from experimental difficulties and from assumptions about the thermodynamic behaviour of the phases involved. We follow the approach adopted by Griffin et al. (1984) by which acceptable P-T values of an assemblage should lie in the experimentally determined field of similar compositions. This approach has been successfully applied to xenoliths from southeast Australia (O'Reilly and Griffin, 1985a, 1985b), Spitsbergen, Norway (Amundsen et al., 1987), southeastern China (Xu et al., 1996) and previously also to xenoliths from western India (Dessai et al., 2004, 2009).

4. Results

The xenoliths from western India vary from dunites to harzburgites to spinel lherzolites. Those from Murud-Janjira show chemical characteristics similar to those from Kutch. They are dominated by olivine which varies from 62 to 85 vol% with Mg# [Mg/(Mg + Fe) atomic] >0.89- > 0.92, CaO less than 0.1 wt%, Ni 3200–4700 ppm, Cr 100–200 ppm. Orthopyroxene (Mg #: 0.89–0.92) in most xenoliths varies from 5 to 20 vol% and it contains Al_2O_3 from 2.38–4.53 wt%, CaO from between 0.52 and 0.98 wt%. Spinel has a modal composition varying from 0.5–3.0 vol%, MgO varies from 15.24–22.04 wt%, Al_2O_3 from 42.74–59.30 wt% and Cr_2O_3 from 7.71–24.45 wt% [Cr# (Cr/Cr + Al atomic) =12.54–17.20]. Mg # of olivine shows positive correlation with Cr # of spinel. Clinopyroxene (Mg#: 0.90–0.91) shows a

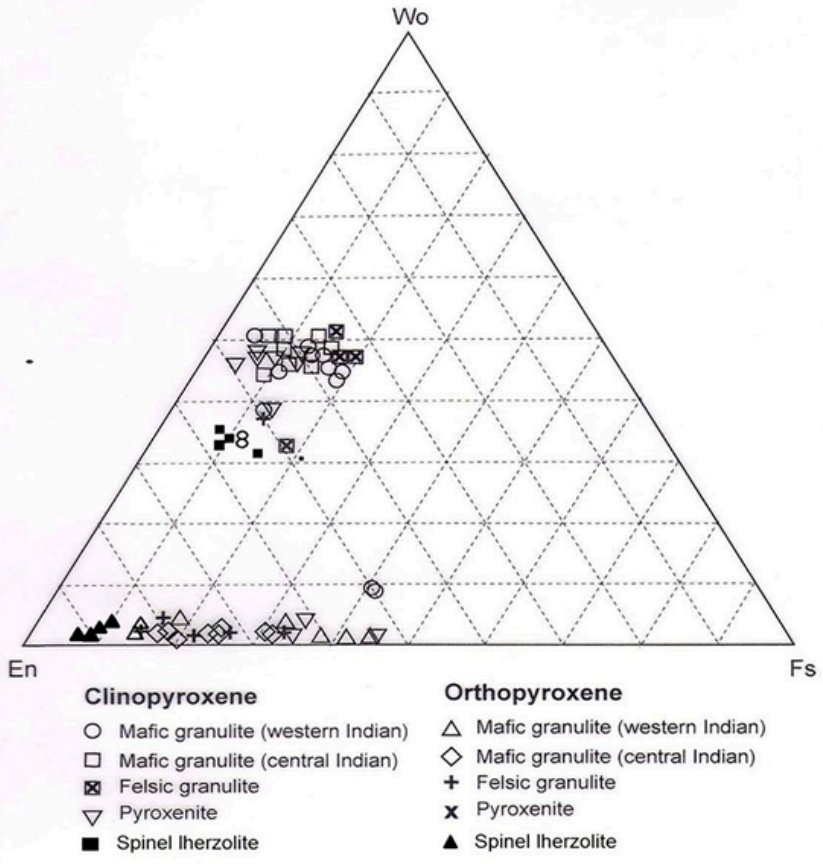

Fig. 4. Compositions of pyroxenes from the xenoliths from present study and those from literature as in Table 1) in the Wo-En-Fs face of the pyroxene quadrilateral.

limited variation from 8 to 15 vol% (Table 2), indicating a low degree of depletion. It shows similarity with Proterozoic xenoliths from the North American craton (Schmidberger and Francis, 1999). Based on the orthopyroxene content, the xenoliths also show compositional similarities with those from Siberia (Boyd, 1989).

The lherzolite xenoliths from Kutch contain olivine with Mg# varying from >0.89- > 0.92. Orthopyroxene shows a limited variation with $Ca_{0.87–1.0}Mg_{89-91}Fe_{10-08}$ with low Al_2O_3 (3–3.5 wt%) except that it is rarely between 1.5 and 2.0% (Karmalkar and Duraiswami, 2010). Clinopyroxene is a chrome diopside with composition Ca_{47-49} $Mg_{48-49}Fe_{5-2}$. CaO and Al_2O_3 show a negative correlation.

4.1. P-T Estimates

Equilibration temperatures (Table. 3) of peridotites (harzburgite/dunites and spinel lherzolites) using the Wood and Banno (1973) calibration are between 1025 and 1114° C and are higher by 60-90° C than those by the Brey and Kohler (1990) and Putirka (2008) calibrations. These are treated as significant considering the mineral-micromorphology (high Al/Ca- cores of pyroxenes) (Dessai et al., 1990; Karmalkar et al., 2000) and the earlier high-temperature history of the spinel peridotites. High T values are also provided by the Sachtleben and Seck (1981) and Witt-Eickschen and Seck (1987) geothermometers. The calibration of Wells (1977) gives T values that are lower by 90-100° C than those by Wood and Banno (1973) thermometer. Equilibration pressures using the updated calibration of Putirka (2008) provided values of 0.59–1.19 GPa. The granulites yield T values from 967-1095° C by Wood and Banno (1973) calibration; these are higher by 60-100° C than those by the Brey and Kohler (1990) and Putirka (2008) calibrations. The equilibration pressures estimated using the Putirka (2008) geobarometer vary from 0.56–1.39 GPa. Given the absence of plagioclase and garnet in the xenoliths, we conclude that even in those containing clinopyroxene and aluminous spinel, the xenoliths equilibrated at pressures between 1 and 2 GPa (Green and Hibberson, 1970; O'Neil, 1981). The plot of the T-P combination of Wood and Banno (1973) and Putirka (2008) defines a kink in the perturbed western Indian geotherm (Dessai et al., 2004) (Fig. 5 A).

The garnet-xenocryst-based geotherm of the 1 Ga Kalyandurg kimberlite from the western margin of WDC is presented in Fig. 5 B (Griffin et al., 2009). Several other well established geotherms from different parts of the world (Amundsen et al., 1987; Griffin et al., 1979; O'Reilly and Griffin, 1985a, 1985b) and India (Dessai et al., 1999, 2004) are shown for comparison. These geotherms not only provide vital information on the secular variation in thermal regimes of the WDC and the Indian shield in general, but also give a glimpse of the petrological variations corresponding to two different spatial and time bands, namely the Proterozoic from the kimberlite xenoliths and the Cenozoic from the Deccan Traps xenoliths, in the evolution of the WDC.

5. Discussion

We discuss the deformational characteristics and the petrological variation of peridotites on the basis of textural features and mineralogy of xenoliths from this and prior studies. The nature and composition of the mantle rocks are scrutinized based on the mineral chemistry which is followed by the thermal structure of the craton from P-T estimates of xenoliths. Lastly the thermomagmatic evolution of the craton is discussed by integrating the mineralogical, petrological, P-T estimates and the geophysical studies on the WDC.

Table 2
EPM analyses of mantle xenoliths from the Deccan Traps, WDC.

Sample No	Mrd /129				Mrd/121			
Const.wt%	Ol	Opx	Cpx	Spn	Ol	Opx	Cpx	Spn
SiO_2	40.71	56.28	53.51	0.04	40.68	56.22	52.30	0.05
TiO_2	0.02	0.03	0.05	0.04	0.04	0.09	0.19	0.03
Al_2O_3	0.03	2.41	2.69	34.63	0.02	2.38	2.74	34.60
Cr_2O_3	0.01	0.46	0.79	31.12	0.02	0.25	0.56	31.15
FeO	8.56	5.56	2.35	16.48	8.53	5.59	2.30	16.46
MnO	0.15	0.13	0.05	0.00	0.18	0.1	0.22	000
MgO	50.00	34.40	17.00	17.35	49.95	34.6	11.16	17.37
CaO	0.03	0.55	22.89	0.03	0.08	0.65	22.13	0.02
Na_2O	0.00	0.01	0.58	0.01	0.00	0.06	0.24	0.02
K_2O	0.00	0.00	0.00	0.01	0.00	0	0	0.01
NiO	0.44	0.04	0.05	0.26	0.42	0.02	0.04	0.44
Total	99.95	99.87	99.96	99.97	99.93	99.94	99.93	99.95
Mg #	0.91	0.91	0.92	0.65	0.91	0.89	0.90	0.65
Sample No	Mrd/124				Mrd/130			
Const.wt%	Opx	Opx	Cpx	Spn	Opx	Opx	Cpx	Spn
SiO_2	40.57	55.00	52.34	0.04	40.59	55.02	52.04	0.05
TiO_2	0.04	0.03	0.17	0.2	0.02	0.10	0.47	0.11
Al_2O_3	0.02	4.32	6.27	57.78	0.01	4.33	6.23	57.81
Cr_2O_3	0.02	0.26	0.6	9.30	0.02	0.27	0.63	9.00
FeO	10.39	6.61	2.9	11.73	10.41	6.60	2.94	11.74
MnO	0.15	0.12	0.07	0.02	0.13	0.15	0.09	0.01
MgO	48.30	32.67	15.56	20.84	48.34	32.64	15.24	20.86
CaO	0.09	0.65	20.94	0.03	0.05	0.68	20.92	0.01
Na_2O	0.01	0.09	1.3	0.01	0.01	0.06	1.32	0.01
K_2O	0.00	0.01	0.03	0.00	0.00	0.00	0.01	0.00
NiO	0.36	0.26	0.6	0.37	0.37	0.09	0.04	0.37
Total	99.94	100.02	100.78	99.93	99.95	99.94	99.93	99.97
Mg #	0.89	0.90	0.90	0.76	0.89	0.89	0.90	0.76
Sample No	Mrd/132				Krl/155			
Const.wt%	Ol	Opx	Cpx	Spn	Ol	Opx	Cpx	Spn
SiO_2	43.90	55.88	52.66	0.05	43.89	55.78	52.56	0.04
TiO_2	0.01	0.03	0.16	0.07	0.02	0.13	0.26	0.08
Al_2O_3	0.03	2.97	4.19	42.74	0.03	2.95	4.17	0.03
Cr_2O_3	0.02	0.44	1.16	24.45	0.01	0.43	1.13	0.01
FeO	8.21	5.65	2.49	13.18	8.22	5.67	2.49	8.23
MnO	0.12	0.11	0.07	0.01	0.11	0.10	0.09	0.10
MgO	46.96	34.23	16.30	19.20	46.97	34.24	16.50	46.95
CaO	0.07	0.53	21.91	0.01	0.06	0.52	21.7	0.08
Na_2O	0.01	0.03	0.95	0.01	0.02	0.04	0.98	0.02
K_2O	0.00	0.01	0.01	0.01	0.00	0.02	0.02	0.00
NiO	0.35	0.06	0.07	0.26	0.34	0.02	0.13	0.33
Total	99.68	99.91	99.97	99.99	99.67	99.20	100.01	99.98
Mg #	0.91	0.89	0.92	0.72	0.91	0.92	0.92	0.72
Sample No	Krl/158				Mrd/134			
Const.wt%	Ol	Opx	Cpx	Spn	Ol	Opx	Cpx	Spn
SiO_2	40.42	54.80	51.00	0.03	40.44	54.87	51.13	0.03
TiO_2	0.04	0.19	0.63	0.12	0.02	0.12	0.52	0.11
Al_2O_3	0.01	4.46	6.42	59.22	0.01	4.49	6.32	59.23
Cr_2O_3	0.01	0.25	0.24	7.71	0.01	0.26	0.58	7.71
FeO	10.27	6.63	2.84	11.17	10.29	6.60	2.94	11.19
MnO	0.15	0.1	0.09	0.03	0.13	0.12	0.08	0.02
MgO	48.63	32.73	14.97	21.12	48.65	32.71	14.98	21.14
CaO	0.04	0.66	20.8	0.04	0.02	0.64	20.88	0.02
Na_2O	0.01	0.04	1.38	0.02	0.01	0.06	1.34	0.02
K_2O	0.00	0.01	0.03	0.00	0.00	0.02	0.01	0.00
NiO	0.36	0.11	0.03	0.41	0.36	0.11	0.03	0.42
Total	99.93	100.01	98.81	99.88	99.94	100.00	98.81	99.89
Mg #	0.89	0.89	0.90	0.77	0.89	0.89	0.90	0.78

Sample No	Krl/172				Mrd/174			
Const.wt%	Ol	Opx	Cpx	Spn	Ol	Opx	Cpx	Spn
SiO_2	40.12	55.00	52.14	0.03	40.04	54.82	52.24	0.04
TiO_2	0.04	0.12	0.37	0.12	0.03	0.12	0.27	0.11
Al_2O_3	0.01	4.30	6.33	59.10	0.01	4.53	6.63	59.00
Cr_2O_3	0.01	0.27	0.62	7.78	0.01	0.26	0.61	8.02
FeO	10.17	6.63	2.84	11.23	10.19	6.6	2.54	11.86
MnO	0.16	0.14	0.08	0.04	0.12	0.25	0.08	0.03
MgO	48.93	32.65	15.25	22.04	48.95	32.34	15.23	21.02
CaO	0.04	0.65	20.82	0.03	0.03	0.98	20.70	0.05
Na_2O	0.01	0.09	1.42	0.02	0.01	0.07	1.54	0.03
K_2O	0.00	000	0.01	0.01	0.00	000	0.03	0.01
NiO	0.40	0.15	0.50	0.42	0.42	0.13	0.48	0.40
Total	99.89	100.00	100.38	100.82	99.81	100.10	100.35	100.57
Mg #	0.91	0.90	0.90	0.77	0.89	0.90	0.91	0.77

Sample No	Krl/176			
Const.wt%	Ol	Opx	Cpx	Spn
SiO_2	40.22	53.87	51.00	0.04
TiO_2	0.04	0.12	0.32	0.12
Al_2O_3	0.01	5.49	6.43	59.30
Cr_2O_3	0.01	0.25	0.57	8.04
FeO	10.15	6.50	2.90	11.5
MnO	0.18	0.22	0.12	0.45
MgO	48.96	32.51	16.98	21.14
CaO	0.03	0.84	19.86	0.04
Na_2O	0.02	0.05	1.36	0.03
K_2O	0.00	000	0.012	0.01
NiO	0.04	0.15	0.50	0.45
Total	99.66	100.00	99.55	101.12
Mg #	0.89	0.91	0.94	0.79

Sample No	Krl/148G			Krl/150 G		
Const.wt%	Cpx	Opx	Gnt	Cpx	Opx	Gnt
SiO_2	50.86	53.30	41.47	50.66	53.23	41.46
TiO_2	0.69	0.11	0.10	0.69	0.14	0.12
Al_2O_3	8.08	5.46	22.99	8.12	5.67	23.04
Cr_2O_3	0.25	0.11	0.20	0.25	0.15	0.18
FeO	4.36	9.90	11.70	4.29	9.66	11.40
MnO	0.06	0.12	0.41	0.09	0.13	0.44
MgO	13.87	30.07	17.87	13.93	30.09	18.04
CaO	20.01	0.63	5.15	20.42	0.67	5.28
Na_2O	1.71	0.10	0.04	1.48	0.08	0.01
K_2O	0.02	0.00	0.01	0.00	0.00	0.00
NiO	0.06	0.14	0.03	0.03	0.13	0.01
Total	99.97	99.94	99.97	99.96	99.95	99.98
Mg #	0.85	0.84	0.72	0.87	0.84	0.73

Sample No	Krl/152G			Krl/160 G		
Const.wt%	Cpx	Opx	Gnt	Cpx	Opx	Gnt
SiO_2	49.41	52.49	40.64	49.43	52.48	40.60
TiO_2	0.98	0.23	0.15	0.96	0.24	0.19
Al_2O_3	6.64	4.99	22.58	6.60	4.96	22.56
Cr_2O_3	0.04	0.01	0.03	0.08	0.04	0.05
FeO	6.29	12.79	14.19	6.25	12.80	14.15
MnO	0.16	0.27	0.64	0.20	0.26	0.68
MgO	14.21	28.25	15.78	14.17	28.26	15.76
CaO	21.64	0.86	5.93	21.68	0.87	5.95
Na_2O	0.57	0.02	0.01	0.56	0.02	0.01
K_2O	0.00	0.00	0.00	000	000	000
NiO	0.04	0.04	0.01	0.05	0.04	0.01
Total	99.98	99.95	99.96	99.96	99.95	99.96
Mg #	0.80	0.79	0.66	0.66	0.79	0.66

Sample No	Krl/168 G			Krl/170 G		
Const.wt%	Cpx	Opx	Gnt	Cpx	Opx	Gnt
SiO_2	50.52	53.10	40.62	49.03	52.9	40.60
TiO_2	0.68	0.10	0.17	0.94	0.21	0.17
Al_2O_3	8.93	5.57	22.54	7.02	5.90	22.58
Cr_2O_3	0.25	0.42	0.07	0.45	0.43	0.05
FeO	4.32	9.80	14.20	4.12	9.60	14.10
MnO	0.1	0.22	0.63	0.1	0.25	0.69
MgO	14.87	29.97	15.73	15.07	30.00	15.79
CaO	19.01	0.73	5.98	18.71	0.70	5.90
Na_2O	1.72	0.10	0.01	1.82	0.13	0.06
K_2O	0.01	0.00	0.00	0.01	000	000
NiO	0.04	0.04	0.01	0.05	0.04	0.01
Total	99.98	99.95	99.96	99.96	99.95	99.96
Mg #	0.80	0.79	0.66	0.66	0.79	0.66

Ol: olivine Opx: orthopyroxene Cpx: clinopyroxene Gnt: garnet Spn: spinel (spinel lherzolites:Mrd/121, Mrd/124, Mrd/129, Mrd/130: 18 °.1859 N 72 °.5738 E,; Mrd/132, Mrd/134: 18 °.3000 N, 72 °.9667 E; mafic granulite: Krl/148, Krl/150, Krl/152, Krl/160, Krl/ 168, Krl/170 and spinel lherzolite: Krl/155, Krl/158: 18 °.5363 N, 72 °.9. First 11 samples are peridotites, last 6 are mafic granulites shown with suffix G, Mrd: Murud-Janjira; Krl: Borlai-Korlai ~10 km north of Murud-Janjira, Mg#: Mg/(Mg + Fe).

Table 3
P-T estimates of Mantle xenoliths from the Deccan Traps, WDC.

Sr. No.	Smpl. No.	Wells (1977) ° C	Brey and Kohler (1990) ° C	Putirka (2008) ° C	Wood and Banno (1979) ° C	Putirka (2008) GPa
1	Mrd/129	906	851	920	1025	0.59
2	Mrd/130	942	947	948	1040	0.99
3	Mrd/132	927	900	953	1045	0.90
4	Mrd/134	920	911	939	1023	0.99
5	Mrd/ 120	913	962	1101	1017	0.95
6	Mrd/121	922	904	920	1029	1.08
7	Mrd/124	947	950	953	1046	1.12
8	Krl/155	943	920	963	1059	0.9
9	Krl/158	915	903	920	1018	0.89
10	Mrd/166	949	971	926	1069	1.19
11	Mrd/172	939	940	947	1038	1.07
12	Mrd/174	940	945	952	1039	0.83
13	Mrd/176	1018	1027	1014	1114	1.04
14	Mrd/148 G	928	926	938	1095	1.31
15	Mrd/150 G	928	925	939	997	1.13
16	Mrd/152 G	918	925	939	989	1.2
17	Krl/160 G	923	884	945	967	0.56
18	Mrd/168 G	1015	1022	986	1067	1.39
19	Mrd/170 G	994	977	995	1054	1.33

1–13 peridotites, 14–19 Mafic Granulites.

In any assessment of seismic structure of the lithosphere, information on two factors is essential. They are: (i) the petrological variation with depth and (ii) the thermal state of the lithologies and its variability. Most other physical parameters of the lithological types, measured by geophysical techniques, are governed, by the mineralogy, and homogeneity of the rocks, which in other words refers to 'packing'- the fabric of the rocks, both intrinsic and superimposed, and the presence of fluids. The other guiding factor controlling physical parameters is the temperature distribution, which is partly governed by the concentration of HPEs (heat producing elements) of the rocks and partly by the thermomagmatic events witnessed by the region during the course of its evolution.

5.1. Textural Features and Deformation

Based on the xenolith suite the cratonic mantle beneath WDC can be classified into two petrological types namely (i) coarse-grained peridotites which have predominantly refractory compositions and (ii) finer-grained sheared peridotites which have more fertile compositions. Both provide similar ranges of equilibration temperatures. The gradational nature of microstructures such as porphyroclastic texture with intracrystalline deformation features such as undulose extinction, subgrain boundaries in olivine, and kink bands in orthopyroxene provide evidence of deformation by dislocation creep (Boullier and Nicolas, 1975; Drury and van Roermund, 1989). They correspond to domains that may have been less annealed due to residence in shallower and cooler parts of the mantle or from less metasomatized parts of the mantle keel. Alternatively, they may have undergone deformation shortly before xenolith entrapment. The first interpretation of shallow derivation seems more appropriate since low equilibration temperatures may favour preservation of deformation microstructures for a long time subsequent to the cessation of deformation (Drury and van Roermund, 1989).

The strong penetrative foliation of olivine and orthopyroxene suggests deformation in the lithospheric mantle beneath the region, whereas the well-equilibrated microtextures are indicative of recrystallisation during deformation at low strain rates and high temperature. Most mineral phases display resorbed spongy rims (Griffin et al., 1979; Rogers, 1977) suggesting either reaction with infiltrated fluids or reheating during transport (Lee and Rudnick, 1999). However, the latter possibility is more probable, as the rims are not confined to mineral phases from any specific depth range but are displayed by all mineral phases of the entire lithospheric section. Spinel-pyroxene intergrowths are quite common and are indicative of garnet destabilization, as also described from several cratons including the North Atlantic craton, West Greenland (e.g. Aulbach et al., 2017b).

Polygonal olivine and orthopyroxene free from deformation imply an earlier higher- stress deformation episode that was followed by the development of mosaic textures indicative of effective recovery and annealing recrystallization of the mantle peridotites under static conditions; they may represent vestiges of the cratonic keel. This may have been associated with fluid-induced grain- boundary migration (Baptiste et al., 2012) during several post-kinematic episodes of modal and cryptic metasomatism (Dessai et al., 1990; Karmalkar et al., 2005) leading to the formation of clinopyroxene and phlogopite that are free of deformation.

The timing of the metasomatic episode is not precisely known, but may have occurred subsequent to the last deformational episode and prior to the entrainment of xenoliths in the lamprophyres, which have been dated by Ar—Ar techniques to 65.2+ 0.4 Ma (Hofmann et al., 2000). This approximately coincides with a ridge jump at 66 Ma (MacKenzie and Sclater, 1971; Norton and Sclater, 1979) and the end of the strongest phase of Deccan magmatism. It post-dates the initiation of India-Seychelles rotation in Mascarene basin by approximately

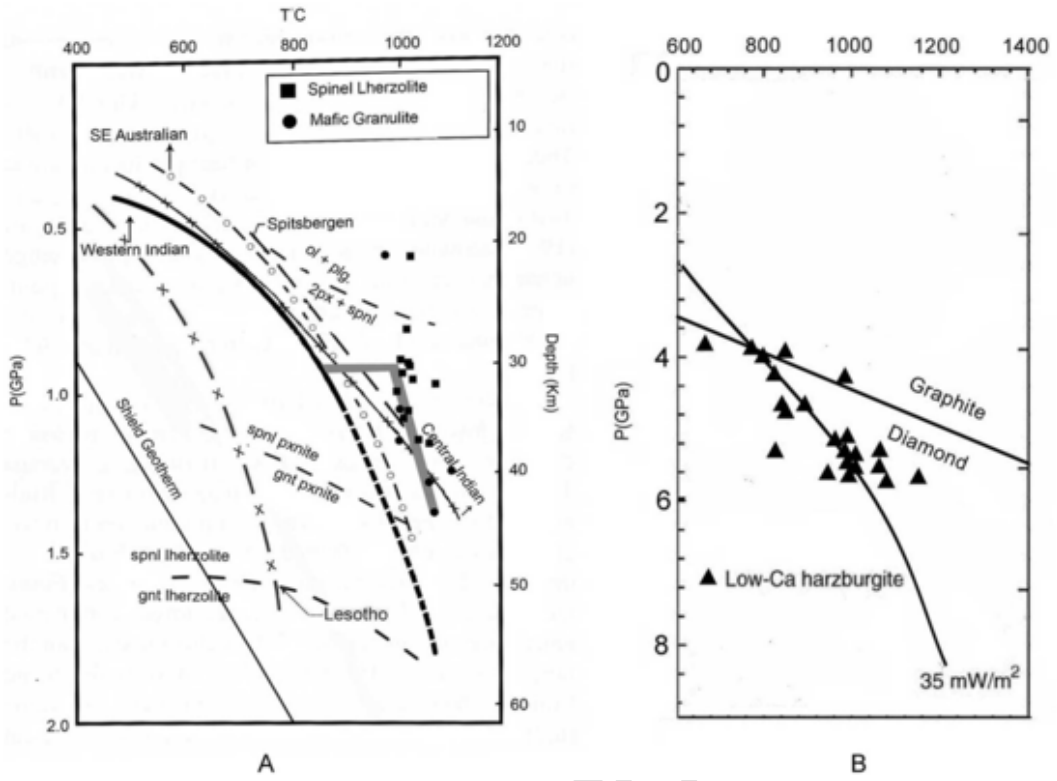

Fig. 5. A. Empirical palaeogeotherms for WDC constructed from geothermobarometry of spinel lherzolite xenoliths following the Wood and Banno (1973) geothermometer and Putirka (2008) geobarometer. The western Indian and central Indian xenolith-based geotherms (Dessai et al., 2004; 2009) are presented. The present geotherm (light grey) represents a kink on the western Indian geotherm of Dessai et al. (1999, 2004). This deflection in the geotherm is justified as seen from high Al/Ca in cores of pyroxenes (Dessai et al., 1990; Karmalkar et al., 2005) and indicates the earlier thermal impress witnessed by the xenoliths. The southeast Australian [(SEA) O'Reilly and Griffin, 1985], Lesotho (Griffin et al. (1979), and Spitsbergen geotherms are presented for comparison. The shield geotherms is schematic. B. Garnet geotherm (after Ryan et al., 1996) proposed for the 1 Ga Kalyandurg kimberlite which intruded the SCLM of WDC and EDC through the high-angle east-dipping sutured contact between the two cratons (Chadwick et al., 2000; Griffin et al., 2009; Kaila et al., 1979).

19 Ma (Storey et al., 1995) implying post-deformational magmatism. Several magmatic episodes are recognized along the western margin.

5.2. Nature of the SCLM beneath Western India

The xenoliths from the western margin both from Murud-Janjira and Kutch show similarities to both Archaean and Proterozoic/Phanerozoic lherzolites. A clear-cut categorization, either as high-Mg# or low-Mg# type (e.g. Boyd and Mertzman, 1987) is not possible, adding to the complexity of the mantle (e.g. Walter, 1998). This is also depicted in the plot of Mg# versus modal olivine (Fig. 6) (e.g. Boyd, 1989; Griffin et al., 2003) in which the lherzolite xenoliths, from the WDC define a crude trend, whereas those from Kutch (Karmalkar et al., 2000), scatter broadly within the field of Proterozoic lherzolites. A few of the xenoliths, with high Mg# (0.90- > 0.91), have 3400–4200 ppm Ni, less than 0.1 wt% CaO and less than 0.03 wt% Al_2O_3, more refractory than typical primitive mantle compositions (e.g. Gaul et al., 2000; McDonough and Sun, 1995) suggesting high degrees of depletion in basaltic components (e.g. Bernstein et al., 1998). Very limited variability in the Mg# of olivine (0.89–0.91), orthopyroxene (Mg#: 0.89–0.92) but considerably larger variation in the Cr# of spinel (0.12–0.53) is seen within the suite as a whole. A good positive correlation is observed between Mg# (0.90- > 0.91) of olivine and Cr# (0.36–0.47) of spinel in coexisting olivine-spinel pairs in depleted rocks. These variations can be interpreted as resulting from partial melting and melt related metasomatism (Gaul et al., 2000) of the lower portions of the lithosphere, consistent with the pressure estimates. Clinopyroxenite veins provide evidence of melt intrusion into the host peridotites after the deformation and melting events. However, some xenoliths show similarities with garnet lherzolites from the Kaapvaal craton and with low-clinopyroxene (<20%) peridotites from Tanzania and Greenland in having low modal clinopyroxene and spinel, moderate to high orthopyroxene/olivine, high Cr # and enrichment of

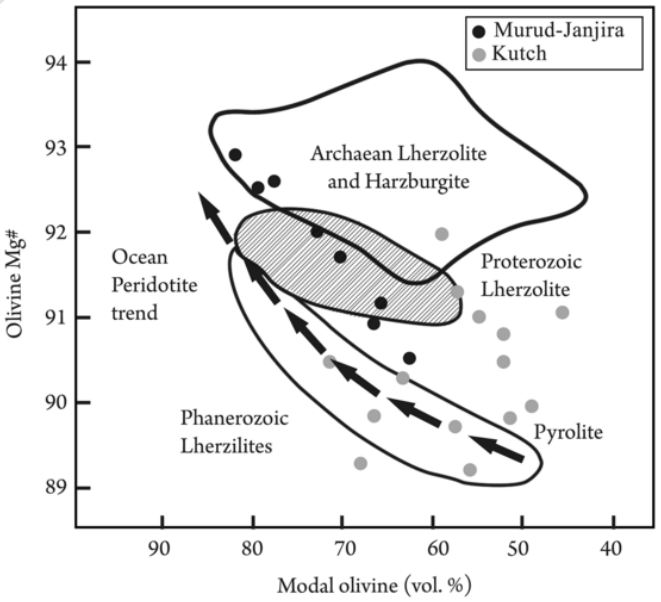

Fig. 6. Plots of xenoliths from Murud-Janjira and Kutch, western India showing compositional trends for upper mantle peridotites from different tectonic settings (modified after Boyd, 1989; Griffin et al., 2003). Oceanic trend (op. cit.) and ranges for the Archaean, Proterozoic and Phanerozoic lherzolites are depicted for comparison.

trace elements in clinopyroxene (e.g. Bernstein et al., 1998; Rudnick et al., 1994). The most depleted of the Kutch xenoliths have been interpreted as relict Archaean lithospheric mantle; their high Mg # at a given Cr # of spinel also categorises them as cratonic peridotites (e.g. Griffin et al., 1999; Karmalkar et al., 2000).

However, Nd—Sr isotope ratios of xenoliths from Kutch have been interpreted in terms of mixing between Reunion mantle and continental lithosphere (Fisk et al., 1988; Simonetti et al., 1998). The isotopic and chemical variations may suggest that the Kutch rocks did not acquire the geochemical signatures merely from an asthenospheric OIB source; an additional source, possibly similar to shallow asthenosphere with a MORB-source geochemical signature may have been involved (Karmalkar et al., 2005). Isotopic studies on perovskite xenocrysts in the Proterozoic kimberlites show $\varepsilon Nd_{(T)}$ values 2.1 ± 0.6 to 6.7 ± 0.3 consistent with a depleted mantle, whereas the Cretaceous kimberlites have pervoskites with lower $\varepsilon Nd_{(T)}$ values - 6.3 ± 1.3 (Chalapathi Rao et al., 2015). Thus, involvement of a depleted and re-enriched source is indicated in the generation of the Phanerozoic (66.7 ± 0.8 Ma; Lehmann et al., 2010) kimberlites.

5.3. The Thermal Boundary Layer

The results of the lithospheric studies on Indian cratons have generated two sets of opinions. A *ca* 200 km-thick lithosphere was estimated by various geophysical techniques (Gupta et al., 1991; Gupta et al., 2003; Maurya et al., 2016; Mitra et al., 2006; Roy and Rao, 2000; Singh et al., 2014) with a fairly thick low-velocity horizon (~50 km) at 50–100 km depth. A thinner (<100 km) and denser lithosphere has been proposed based on other geophysical techniques (Borah et al., 2014a, 2014b; Gokarn et al., 2004; Kumar et al., 2007b, 2013; Negi et al., 1986, 1987) implying the absence of thick lithospheric roots. The results of these studies are not complementary owing to differences in resolution and the assumptions made in employing the preferred model. The petrological composition of the lithosphere-, can help to improve lithosphere thickness estimates.

The mantle xenoliths constrain the lithospheric thickness and the thermal state of the mantle at the time of host-lamprophyre intrusion at *ca* 65 Ma (Hofmann et al., 2000). The xenoliths from the Kutch show equilibration temperatures of 884-972° C whereas those from Murud-Janjira are in the range of 1025-1114° C and 0.59–1.19 GPa. The associated granulites show equilibration temperatures of 967-1095° C and 0.56–1.39 GPa (Dessai et al., 1999, 2004). The pressure estimates make it clear that mafic granulites extend much below the seismic Moho discontinuity into the spinel lherzolite (original harzburgites/dunites) stability field of the shallow lithosphere in this region. The inter-stratification of granulites with the ultramafic rocks implies magmatic accretions that under- and intra-plated the crust-mantle transition zone, leading to lithospheric growth and a deeper petrological crust-mantle boundary beneath this region (Dessai et al., 2004, 2009).

The low temperatures of the Kutch xenoliths indicate their entrainment from shallow depths (Karmalkar et al., 2000) while those from Murud-Janjira came from deeper levels provided they equilibrated to a conductive geotherm. The equilibration pressures derived from the western continental margin geotherm (Dessai et al., 2004) indicate depths of 40–50 km for the Kutch xenoliths and about 45–55 km for those from Murud-Janjira. These estimates suggest that the xenoliths resided at these depths prior to their entrainment in the host magma. Many of them have retained an early high-temperature history recorded in high Al and/or Ca in the cores of pyroxenes. As noted above, such relict minerals yield higher equilibration temperatures.

The xenoliths from the present study indicate high mantle adiabat along an 80–90 mWm^{-2} conductive geotherm indicating transient advective heating. They occupy a field analogous to other regions of Cenozoic extension, rifting and volcanism such as North China, Siberia, Spitsbergen. Assuming that the ambient mantle adiabat is representative of the convective upper mantle, the intersection of the xenolith geotherm with the mantle adiabat at about 60–80 km corresponds to the lithospheric thickness in this region. These depth estimates are similar to those of Mukherjee and Biswas (1988) and Dessai et al. (2004). This depth range marks a transition, in which a distinct change in the mode of heat transfer occurs, from conductive in shallower regions to convective below ~100 km. This observation also finds support in some geophysical investigations, but the base of the geophysically estimated thermal boundary layer is deeper by about 50 km than the xenolith-defined layer (Gokarn, 2003).

A comparison of different cratons is depicted in Fig. 5A. The Western Indian geotherm (Dessai et al., 1999, 2004) derived from xenoliths in lamprophyres implies temperatures higher than those normally expected from conductive cooling of the craton and suggests a maximum lithospheric thickness of ~145 km during Proterozoic time. A note of caution is essential: such thickness estimates should be done on the basis of steady-state geotherms which is not the case for the WDC. The western Indian geotherm (Dessai et al., 2004) is cooler by about 50-100° C than the southeast Australian one, but distinctly hotter than that of Lesotho (Ganguly and Battacharya, 1987; Griffin et al., 1979). The xenocryst- derived EDC geotherm (Griffin et al., 2009) from the Kalyandurg pipe that penetrated the WDC-EDC contact, provides a maximum lithosphere thickness of about 175–185 km during Proterozoic. Thus, during Proterozoic time itself the WDC recorded a distinct variation in lithospheric thickness (~30–40 km) between its western and eastern margins. This difference increased further to nearly 90–100 km, due to thermomechanical erosion attendant on the DT magmatism.

The spinel lherzolite xenoliths from the present study, however, show a distinct kink (inflexion) in the Western Indian geotherm (Fig. 5). This is indicative of a transient thermal episode during the Palaeocene that heated the base of the depleted lithosphere (e.g. Griffin et al., 2009). It is a reflection of the emplacement of ultramafic melts into the SCLM attendant on the terminal episode represented by the alkaline magmatism of the DT. It also represents the metasomatic activity witnessed by the SCLM (ibid.). The departure of the xenolith P-T estimates from the conductive geotherm may be interpreted as defining the basal part of the upper mantle layer that normally exhibits a conductive heat transfer regime. Such high temperatures are generally interpreted in terms of reduced viscosity and asthenopheric flow, which suggests that the thickness of the thermal boundary layer may not have exceeded ~150 km.

The distinctive nature of the thin thermal lithosphere is also explicit from the similarity of the lithosphere thickness estimates by different techniques and from a comparison between and among cratons from the Indian shield (Table 4).

A cross-validation of the inference drawn from the xenolith-based geotherm is also seen from the heat flow-based geotherm (reference geotherms; Pollock and Chapman, 1977). The mantle xenoliths from the western part of WDC define a hot mantle palaeo-geotherm corresponding to a model geotherm of more than 80 mWm^{-2} (ibid.) (Fig. 7) whereas the Proterozoic geotherm (Griffin et al., 2009) along the eastern margin is 35 mWm^{-2}. The present-day measured heat flow of 29–32 mWm^{-2} (Roy and Mareschal, 2011) suggests a cooler geotherm in the southern and eastern parts of the craton. This geotherm is nearly analogous to the Proterozoic geotherm of the EDC (op. cit.) and is lower than the continental/shield geotherm from other cratons (36–40 mWm^{-2}; Griffin et al., 1992, 1999). The low heat flow could be influenced by groundwater circulation (e.g. Foulger, 2007); alternatively, it could represent a steady-state geotherm attained post-Proterozoic magmatism (Hall et al., 2007). This is indicative of the change in thermal structure from Proterozoic to Phanerozoic. The low geotherm

Table 4
Depth Estimates of LAB (km) for the Chemical-, Thermal-, Seismic- and Electrical-Lithosphere beneath WDC and other Indian cratons based on thermal and non-thermal data.

Precambrian craton	Cratonization Age (Ga) [15, 16, 17]	Chemical Lithosphere (Xenoliths) [1,2,7]	Thermal Lithosphere (Xenolith P-T)	Seismic Lithosphere (RF function) [4]	Electrical Lithosphere (MT) [5]
WDC	3.3–3.0	60–80 [1 $]	~80–100 [$]	<100 [13, 18]	70–160 [5, 19]
EDC	2.7–2.5	175–190 [2]	~175 [3,10]	175–200 [4,9]	~180 [5]
Bastar	~1.8	130–140 [7]	~175 [3,10]	140–200 [8]	–
Bundelkhand	2.6–2.5	65–85 [1]	–	200–250 [8]	–
Aravalli	2.6–2.5	–	160–200	–	–
Singhbhum	3.0–2.5	–	160–200	70–100 [6]	58–95 [6,11]
SGT	2.6–2.5, 2.3	–	180–230	165–180 [12]	–
Western Margin	–	–	–	80–100 [13]	–
Eastern Margin	–	–	–	77–127 [14]	–

1: Dessai et al., 2004; 2: Griffin et al., 2009; 3: Artemieva and Mooney, 2001; 4: Gupta et al., 2003; 5: Gokarn, 2003, Gokarn et al., 2004; 6: Shalivahan et al., 2014; 7: Babu et al., 2009; 8: Maurya et al., 2016; 9: Oreshin et al., 2011; 10: Gupta et al., 1995; 11: Manglik and Mandal, 2016; 12: Singh et al., 2014; 13: Kumar et al., 2007b, 2013; 14: Srinivas Rao et al., 2014; 15: Meert et al., 2010; 16: Jayananda and Peucat, 1996; 17: Krogstad et al., 1991; 18: Borah et al., 2014b; 19: Abdul Azeez et al., 2015; [$]Dessai (this study).

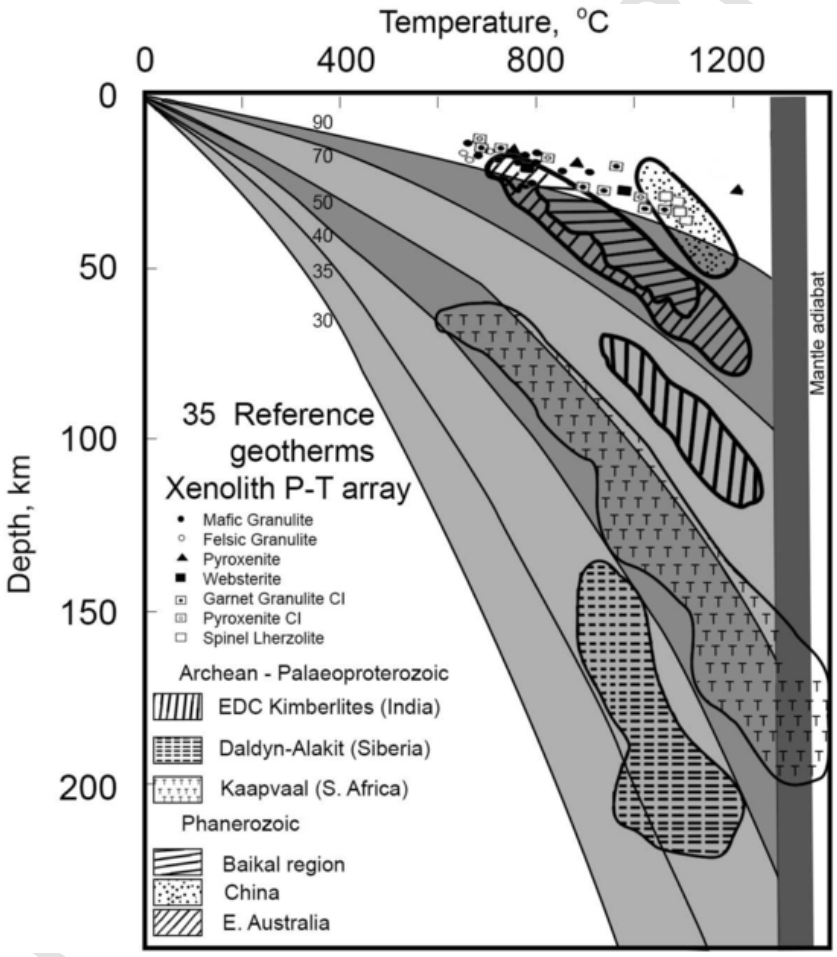

Fig. 7. Comparison of P-T arrays of xenoliths from the Deccan Traps region of the WDC, with the kimberlite xenoliths from EDC and other localities worldwide in reference geotherms of Pollack and Chapman (1977) and typical continental geotherms modelled from heat flow data (modified after Artemieva, 2006).

is reminiscent of the Palaeozoic geotherm of the North China craton (Griffin et al., 1998; Xu et al., 2008).

The 80 mWm $^{-2}$ palaeogeotherm (~65 Ma) suggests a lithosphere thickness of barely about 60–80 km as against a pre-Proterozoic thickness of 145 km. This could be interpreted such that the thermal structure of the WDC has undergone a change from Proterozoic until about 65 Ma ago and is still different than the present-day situation. The present-day heat flow of the craton is much less than the average global heat flow (~64 mWm^{-2}). However, a prominent heat flow anomaly (Gupta, 1982) with values ranging from 65 to 100 mWm^{-2} (Gupta and Gaur, 1984; Roy and Mareschal, 2011) defines western India (Cambay). This a reflection of the Cenozoic thermal transient on the lithosphere of the western Indian margin also reflected in the high equilibration T of spinel peridotites xenoliths by the Wood and Banno (1973) calibration. It suggests that the advective heat has not yet reached the surface in the eastern part of the craton where the lithosphere is much thicker than along the craton margin in the west, indicating in turn that the measured heat flow is not a decayed remnant of DT activity. For a lithospheric palaeothickness of ~145 km (pre-Ceno-

zoic) in the west and 175–185 km in the east during Proterozoic, the time required for the thermal effects to reach the surface and be reflected in surface heat flow is usually related to the age of the hotspot and may require more than 100 Ma (e.g. Chapman and Furlong, 1992).

5.4. Chemical Boundary Layer

The SCLM defined on the basis of the chemical composition may not be significantly different from the thermal boundary layer discussed above since depth estimates are based on xenolith data. However, the variation in mineral chemistry does serve to show the variation in bulk composition with depth as well as the antiquity of the mantle chemical stratigraphy. Such an exercise for the xenoliths from the WDC indicates that the depth of the CBL is less than about 100 km (Fig. 8) in the west whereas it is more than about 175 km along the eastern margin of the craton (Kalyadurg Section) and increases further still within the EDC (Ganguly and Battacharya, 1987; Griffin et al., 2009). The depth estimates for the WDC need be taken with caution since they are not based on garnet-facies peridotites as in the neighbouring cratons. However, the symplectic intergrowths of pyroxene-spinel do indicate the presence of former garnet in these xenoliths. Garnet stabilisation due to thinning of the lithosphere, as observed in SW Greenland (Aulbach et al., 2017b) is a distinct possibility.

It has been observed globally that olivine Mg # generally, decreases with depth in most Archaean and Proterozoic cratons. Within the constraints of the data, it could be suggested that a similar decrease is also seen in the Indian cratons. Broadly, in the Archaean cratons at depths of ~100 km the Fo content of olivine shows maximum values of 93 which decreases progressively to 92 at ~120–170 km and attains a value of 88–90 at ~210–240 km. The depth regions where olivine attains primitive mantle values of 88–90 could be interpreted as the base of the CBL or the base of the petrologic lithospheric mantle (Artemieva and Mooney, 2001). This change is noticed at ~210–240 km beneath many Archaean regions and at much shallower depths ~160 km in Proterozoic terrains (Griffin et al., 2009). In this respect, based on the present xenolith suite, the WDC SCLM, is thinner compared to the typical Proterozoic SCLM. It is closely similar both in terms of the degree of depletion and depth to that of eastern Australia and southeast China.

The pattern of decreasing Fo within a narrow depth range is, however, observed only in certain terrains such as the Kaapvaal and Siberian cratons. In Kaapvaal craton for instance, the younger kimberlites (emplaced after 90 Ma) exhibit different Mg # below a depth of ~175–200 km than the older kimberlites (emplaced prior to ~110 Ma). It can be inferred therefore, that subsequent to the intrusion of the older kimberlites the mantle beneath Kaapvaal craton was subjected to metasomatic modification (Kobussen et al., 2009). Such a chemical variation is also exhibited by the WDC mantle (Dessai et al., 1990; Karmalkar et al., 2005) and also holds good for the adjoining EDC (Griffin et al., 2009).

5.5. Tectonic Reactivation and Decratonization

The most significant result that ensues from this study is the secular variation in the lithospheric thickness from the Proterozoic to Palaeocene as a consequence of the change from a cratonic (37 mWm^{-2}) to an oceanic (>80 mWm^{-2}) geotherm. Whether this thinning is related to various rifting and partial melting episodes or whether it is related solely to the peak of Deccan magmatism, is debatable and will have to await additional data. Lithospheric thinning from Deccan magmatism was suggested by Peng and Mahoney (1995) on the basis of a progressive N-S trend of decreasing incompatible element patterns in the DT lava pile. Kerr (1994) correlates the lithospheric thinning in Large Igneous Provinces with an increase in the degree of sublithospheric partial melting, possibly moving from garnet peridotite to spinel peridotites facies accompanying thermomechanical erosion of the lithosphere by the relevant plume (Stewart and Rogers, 1996). Although the involvement of a plume in the generation of the DT is widely accepted, an alternative mechanism of delamination of the SCLM (Smith, 1993) could be another possibility.

Tectonic reactivation of the Indian shield in general, and the WDC in particular, commenced in the Proterozoic with the emplacement of Proterozoic dyke swarm dated to 2367 + 1 Ma (Hall et al., 2007). The presence of rocks of adakitic chemistry in the sub-Deccan xenolith suite supports the above proposition whereas the granitic rocks find their equivalents in the abundant lower-crustal felsic granulite xenoliths (SiO_2: 70 wt%; Na_2O/K_2O: >4%; Y/Nb: > 1.2) (Dessai et al., 2004). The intrusion of kimberlite magmas across the WDC-EDC thrust contact in the east implies reworking in late Mesoproterozoic (ca.1.1. Ga) with the intrusion of kimberlite magmas (between 1053 and 1155 Ma) as a consequence of the presumed mantle plume beneath the supercontinent Rodinia (Anil Kumar et al., 2007b). The Proterozoic saw the intrusion of mafic dyke swarms and produced transient heating leading to metasomatic refertilization and densification of the lithosphere of the WDC, aiding its convective removal, as for instance in the case of Wyoming craton and North China craton (Foley, 2008). Reactivation continued through Mesozoic and Cenozoic time. The subcontinental lithospheric mantle (SCLM) may have decoupled from the lower crust around post-Middle Jurassic- late Oxfordian (158 Ma) time

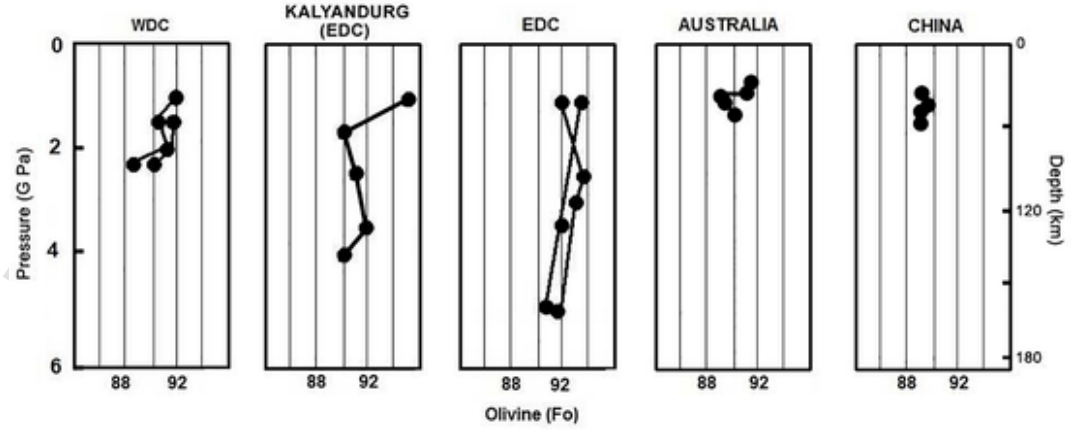

Fig. 8. Mantle chemical variation depicted by the mean Fo content of mantle olivine as a function of depth at the western margin during Palaeocene; at the eastern boundary of WDC-EDC (as exemplified by the garnet xenocrysts from the Kalyandug kimberlite) at 1 Ga; compared to the Fo content observed in the interior of the EDC, (Griffin et al., 2009), eastern Australia and southeast China.

(Courtillot et al., 1986; Storey et al., 1995). This also could be inferred from the Nd—Sr isotope array of the DT, which has been attributed to mixing between juvenile mantle and continental lithosphere (Fisk et al., 1988; Peng and Mahoney, 1995; Simonetti et al., 1998) beneath the western part of the craton, suggesting strong interactions between the asthenosphere and the lithosphere (both upper mantle and lower crust) in Phanerozoic times and heating the western part of the craton more than the eastern.

The chemical transition from a depleted harzburgite composition to a refertilized/metasomatised high-T lherzolitic composition at a shallow depth produces a lower seismic velocity and a sharp increase in density. In a recent seismic reflection profile (Chikmagalur-Perur; Mandal et al., 2018) the easterly-dipping reflection fabric can be interpreted as the vestiges of the Archaean-Proterozoic lithosphere layering, although it has been interpreted as a subduction zone (Mandal et al., 2018).

Other geophysical observations support the lithosphere-thickness estimates. The crust thins to 18–21 km to the north of Mumbai (Kaila, 1988; Kaila et al., 1981), and the sub-Moho seismic velocities (Vp) beneath the craton are less than 8.2 km/s (Vs: 4.5–4.6 km/s) (Battacharya et al., 1992; Kiselev et al., 2008), lower than those beneath the EDC (8.5–8.6 km/s). The lower-crustal Vp/Vs ratios are lower (1.65–1.76) (Rai et al., 2005) than those (1.84) typical for the shields and platforms (Zandt and Ammon, 1995). However, this could be due to the higher Mg#s of mafic granulites (Christensen, 1996), the effect of the high thermal gradient and the heterogeneity of the deep crust.

The electrical structure of the lithosphere shows a conductive layer in the depth range of 60–250 km (Patro and Sarma, 2009). Similarly in MT transects (E-W) across the craton both in DT-covered areas and further south along 13° N latitude (Mangalore), a conductive zone encountered at ~70–160 km has been interpreted as the lithosphere-asthenosphere boundary (Abdul Azeez et al., 2015;Gokarn, 2003 ; Gokarn et al., 1992). It deepens to 180–190 km beneath the EDC east of the Closepet Granite. The high geothermal gradient in the WDC suggests that the conductor is temperature-related, a factor which is most evident but one that has been neglected in geophysical interpretations. The conductor also coincides with the thickness of the SCLM estimated here. In RF studies low Vs (3.5 km/s, Oreshin et al., 2011) is noted at the latitude of Mangalore (Borah et al., 2014a, 2014b) which coincides with the depth of the MT conductor. The low-velocity horizon at 50–100 km (Maurya et al., 2016; Mitra et al., 2006) almost tallies with the high velocity anomaly of Singh et al. (2014) between 100 and 200 km under the DT. It is more likely that as observed from the xenolith data, this anomaly is primarily related to advective heat maintaining the minerals at temperatures near but still below their melting points (Dessai et al., 1990, 2004, 2009; Karmalkar et al., 2005) and partly to contributions from fluid-induced metasomatic modification of the mantle (Griffin et al., 2009). A drop in the solidus temperature of peridotite yields conflicting seismic-thermal-geochemical depths for the LAB accounting for the various interpretations encountered in geophysical investigations. It may be pertinent to point out that the non-existence of diamondiferous kimberlites in the WDC is in itself a strong indication of a thinner lithosphere (e.g. Boyd and England, 1960; Kennedy and Kennedy, 1976). In comparison, diamondiferous kimberlites occur in great profusion to the east in the EDC and to the north in the Bundelkhand craton.

Low Vs is also observed at the latitude of Kutch in the north and it is attributed to metasomatism attendant on the emplacement of mafic magmas (Kiselev et al., 2008; Kosarev et al., 2013a, 2013b; Replumaz et al., 2004); high geothermal gradient (Mukherjee and Biswas, 1988) could be another reason . Compositional heterogeneity is a further likely cause. Vs is directly proportional to the Mg# and inversely proportional to orthopyroxene content. In the spinel peridotite facies, since garnet is precluded, orthopyroxene is the potential candidate for producing the lower Vs. However, considering the low modal content of orthopyroxene in the xenoliths it may not be the likely cause of low Vs. In our opinion the low Vs is primarily due to high temperatures at shallow depths, coupled with the metasomatized nature of the shallow lithosphere.

The SCLM beneath the WDC, and especially that beneath the Deccan Traps, is characterised by harzburgites/dunites with chrome spinel-orthopyroxene symplectitic intergrowths (indicative of the previous existence of garnet). These xenoliths have low clinopyroxene contents and high Mg# indicative of a depleted nature. Other characteristics include the absence of a sharp Moho discontinuity (Dessai et al., 2004), a strongly layered granulitic/eclogitic lower crust, relatively low seismic velocities in the crustal section, high heat flow, steep geothermal gradient, the existence of a gravity high, a thin Curie crust and a relatively thin lithosphere with a low-velocity zone at depth of ~60–80 km which corresponds to a conductor in MT profiles (Gokarn, 2003; Gokarn et al., 1992). These characteristics are unique to the WDC and do not represent the "larger part of the Indian shield".

These strong evidences are inconsistent with the existence of cold and rigid lithospheric roots beneath the DT as suggested earlier (e.g. Iyer et al., 1989; Mahadevan, 1994). All these features along with the two temporally distinct suites of xenoliths, (depleted and fertile-; Archaean/Proterozoic and Cenozoic), fertile mantle coexisting with Archaean crust and a decrease in lithospheric thickness from east to west permit the inference that the SCLM beneath the WDC was repeatedly perturbed by thermomagmatic episodes (more than four) and was eventually strongly rejuvenated or replaced by fertile noncratonic mantle. Such perturbations are not apparent beneath other cratons of the Indian shield, save perhaps the Bundelkhand and Bastar cratons, represented only by sparser data sets.

The xenolith suite suggests that the Archaean lithosphere beneath WDC may be preserved at the most down to ~100 km depth and its lower portion has been replaced by the Phanerozoic lithospheric mantle (Kosarev et al., 2013a, 2013b) with local intermixing between the two (Fig. 9). This is supported by residual harzburgite/dunite xenoliths, compound xenoliths, co-existence of mafic- and felsic- granulites (and A-type granitic rocks) in the lower crust, a high geothermal gradient, a conductor in MT profiles, low Vs coincident with the depth of MT conductor and a linear +70 mGal gravity anomaly approximately centered over Mumbai and the Cambay region.

The tectono-thermal events that were superimposed during Phanerozoic not only brought about accretion but were also responsible for thermomechanical removal (ibid.) or modal and cryptic metasomatic re-fertilisation (Dessai et al., 1990; Karmalkar et al., 2005) by asthenosphere-derived fluids and melts, of the bottom 80–100 km of the Archaean keel (e.g. Eggler and Furlong, 1991; Griffin et al., 1998).

Instances of lithosphere destruction by thermomechanical erosion from asthenosphere upwelling have been described in other cratons such as the Wyoming, Tanzania, North China and Congo craton (Aulbach, 2019; references therein). These cratons have Archaean magmatic ages, or other indicators of Archaean heritage, but have been reworked during the Phanerozoic.

The reworking mechanism can be primarily attributed to the "top down" delamination of the lithosphere as revealed by the presence of mafic and eclogitic granulites deep into the sub-Moho mantle depths and the formation of anatectic felsic granulites from mafic precursors (Dessai et al., 2004). The "bottom-up" thermomechanical erosion attendant on the rise of asthenosphere and attendant fluids is also evident from the under- and intra-plated nature of the Moho transition zone expressed by compound xenoliths and prominent seismic reflectors.

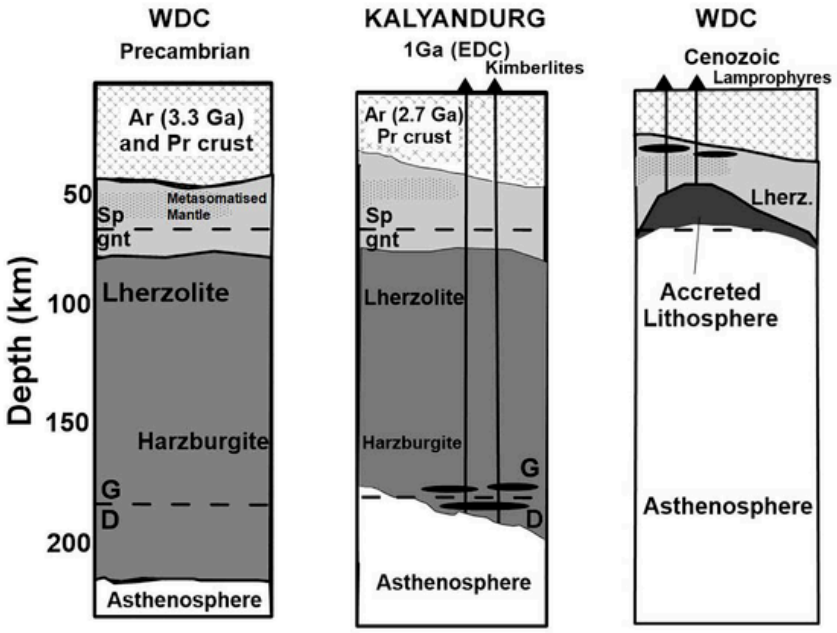

Fig. 9. Secular compositional variation in the lithospheric mantle beneath the WDC from Precambrian (in general) to Mesoproterozoic (1 Ga) especially at the eastern margin (Kalyandurg section) to Cenozoic (65 Ma; at the western margin at Mumbai-Cambay) depicted by means of cartoons based on information from the xenolith. The WDC-SCLM shows distinct temporal evolution both in composition and thickness from the Archaean to the Cenozoic (Ar: Archaean, Pr: Proterozoic, Lherz: Lherzolite, Sp/gnt: Spinel/Garnet, G/D: Graphite/Diamond).

6. Conclusions

The Archaean roots of the Indian shield in general, and the WDC in particular, have been largely compromised in the west; the sole remnants of the tectospheric keel are available beneath the interior EDC. The SCLM beneath the WDC was coupled with the lower crust until Proterozoic and has since been subjected to reworking. Decoupling occurred largely during the Proterozoic attendant on intrusion of mafic dyke swarms (~2.3 Ga) and acquisition of a moderately high thermal imprint. This was followed by a second thermal episode attendant on the Pan-African event (~550 Ma). Greater India's separation from Madagascar at ~91.2 Ma (Torskvik et al., 2000) was responsible for the third thermomagmatic episode. India-Seychelles rotation at ~84 Ma and finally their separation at 66 Ma (Norton and Sclater, 1979) marked the most significant and profound thermomagmatic events witnessed by the Indian shield. It led to delamination ("top-down") as well as thermomagmatic attrition ("bottom-up") episodes resulting in a net loss of more than 100 km of lithosphere thickness suggesting strong interaction between the lithosphere and asthenosphere (both upper mantle and lower crust) during Phanerozoic.

Isobaric cooling of the upwelled asthenosphere during Palaeocene has led to local thickening due to the newly accreted lithosphere, but over the extent of the western margin of the WDC, thermomechanical attrition has resulted in overall thinning of the SCLM from ~175–185 km in the east (east of Closepet Granite) prior to the Proterozoic to 125–145 km to the west (west of Closepet Granite) to ~60–80 km at the western margin beneath (Murud-Janjira) Mumbai-Cambay to barely 40–50 km further west at Kutch. Still further west the relict continental ridges on the ocean floor are almost devoid of crustal sections and have a lithospheric thickness of barely 60 km. Evidence of a thermomagmatic event leading to modal and cryptic metasomatism during Palaeocene suggests that the SCLM beneath western India was rejuvenated by more fertile and noncratonic juvenile mantle, leading to the final decratonisation of the WDC.

Uncited references

Declaration of Competing Interest

The authors declare that they have no known competing financial interests or personal relationships that could have appeared to influence the work reported in this paper.

Acknowledgements

Journal reviews by S. Aulbach and an anonymous reviewer are thankfully acknowledged.

References

Abdul Azeez, K.K., et al., 2015. The electrical resistivity structure across the Dharwar nucleus and Coorg block of south Indian shield: evidence of collision and modified and preserved lithosphere. J. Geophys. Res. 120, 6698–6721.

Amundsen, H.E.F., Griffin, W.L., O'Reilly, S.Y., 1987. The lower crust and upper mantle beneath Northwest Spitsbergen: evidence from xenoliths and geophysics. Tectonophysics 139, 169–185.

Artemieva, I.M., 2006. Global 1o x 1o thermal model TC1 for the continental lithosphere: implications for lithosphere secular evolution. Tectonophysics 416, 245–277.

Artemieva, I.M., Mooney, W.D., 2001. Thermal thickness and evolution of Precambrian lithosphere: a global study. J. Geophys. Res. 106, 16387–16414.

Aulbach, S., 2019. Cratonic lithosphere discontinuities: Dynamics of small-volume melting, meta-Cratonisation and a possible role for brines. In: Yuan, H., Romanowicz, B. (Eds.), Lithospheric Discontinuities. American Geophysical Union, Washington DC, pp. 177–204.

Aulbach, S., Massuyeau, M., Gaillard, F., 2017a. Origins of cratonic mantle discontinuities: a view from petrology, geochemistry and thermodynamic models. Lithos 268–271, 364–382.

Aulbach, S., et al., 2017b. Volatile-rich Metasomatism in the Cratonic Mantle beneath SW Greenland: link to Kimberlites and Mid-lithospheric Discontinuities. J. Petrol. 58, 2311–2338.

Babu, E.V.S.S., et al., 2009. Mantle xenoliths from the Kodomali kimberlite pipe, Bastar craton, central India: evidence for decompression melting and crustal contamination in the mantle source. Geochimica Cosmochimica Acta Suppliment 73 (13), A66.

Baptiste, V., Tommasi, A., Demouchy, S., 2012. Deformation and hydration of the lithospheric mantle beneath the Kaapvaal craton. South Africa. Lithos. doi:10.1016/jlithos.2012.05.001.

Bernstein, S., Kelemen, P.B., Brooks, C.K., 1998. Depleted spinel harzburgite xenoliths Tertiary dykes from East Greenland: Restite from high degree melting. Earth Planet. Sci. Lett. 154, 221–235.

Bhaskar Rao, Y.J., et al., 2008. A review of Paleo- to Neo-archaean crustal evolution in the Dharwar craton, southern India and the transition towards a plate tectonic regime. Episodes 43, 51–68.

Borah, K., et al., 2014a. Complex shallow mantle beneath the Dharwar craton inferred from Raleigh wave inversion. Geophysics Journal International 198, 1055–1070.
Borah, K., et al., 2014b. Seismic imaging of crust beneath the Dharwar craton India from ambient noise and teleseismic receiver modeling. Geophysics Jounal International 197, 748–767.
Boullier, A.M., Nicolas, A., 1975. Classification of textures and fabrics of peridotite xenoliths from South African kimberlites. Physics and Chemistry of the Earth 9, 467–476.
Boyd, F.R., 1989. Compositional distinction between oceanic and cratonic lithosphere. Earth Planet. Sci. Lett. 96, 15–26.
Boyd, F.R., England, J.L., 1960. Apparatus for phase-equilibrium measurements at pressures upto 50 kilobars and temperatures upto 1750 °C. J. Geophys. Res. 65, 741–748.
Boyd, F.R., Mertzman, S.A., 1987. Composition and structure of Kaapvaal lithosphere, South Africa. In: Mysen, B.A. (Ed.), Magmatic Processes: Physicochemical Processes. In: The Geochem. Soc. Sp. Pub, University Park, PA, pp. 13–24.
Boyd, F.R., Nixon, P.H., 1975. Origin of ultramafic nodules from some kimberlites from northern Lesotho and the Monastery Mine South Africa. Physics and Chemistry of Earth 9, 431–445.
Boyd, F.R., Gurney, J.J., Richardson, S.H., 1985. Evidence for a 150-200 km Archaean lithosphere from diamond inclusions thermobarometry. Nature 315, 387–389.
Brey, G.P., Kohler, T., 1990. Geothermobarometry in four phase lherzolite II: new theromobarometers and practical assessment of existing thermobarometers. J. Petrol. 27, 1353–1358.
Burke, K., Dewey, J.F., 1973. Plume generated triple junctions: Key indicators in applying plate tectonics to old rocks. J. Geol. 81, 406–433.
Chadwick, B., et al., 1992. The Dharwar Supergroup: basin development and implications for late tectonic setting in western Karnataka, southern India. In: Glover, J.E., Ho, S.E. (Eds.), The Archaean Terrains, Processes and Metallogeny, 22. Univ. of Western Australia Publ, pp. 3–15.
Chadwick, B., Vasudev, M.N., Hegde, G.V., 2000. Dharwar craton southern India, interpreted as the result of late Archaean oblique convergence. Precambrian Res. 99, 91–111.
Chalapathi Rao, N.V., et al., 2015. A late cretaceous (*ca* 90 Ma) kimberlite event in southern India: implications for sub-continental lithospheric mantle evolution and diamond exploration. Gondw. Res.. doi:10.1016/j.gr.2015.06.006.
Chapman, D.S., Furlong, K.P., 1992. Thermal state of the continental lower crust. In: Fountain, D.M., Arculus, R.J., Kay, R.W. (Eds.), The Continental Crust. Elsevier, Amsterdam, pp. 129–199.
Chardon, D., Jayananda, M., Chetty, T.R.K., Peucat, J.-J., 2008. Precambrian continental strain and shear zone patterns: south Indian case. J. Geophys. Res. 113, B08402. doi:10.1029/2007JB005299.
Chevrot, S., Zao, I., 2007. Multiple finite frequency Railegh wave tomography of the Kaapvaal craton. Geophysics Journal International 169, 201–215.
Christensen, I., 1996. Poisson's ratio and crustal seismology. J. Geophys. Res. 101, 3139–3156.
Coleman, R.G., et al., 1965. Eclogites and eclogites: their differences and similarities. Bullutin Geological Society of America 76, 483–508.
Courtillot, V., et al., 1986. Deccan flood basalts at the cretaceous Tertiary boundary: past climatic crises as a key to the future. Palaeogeology Palaeclimatology and Palaeoecology 89, 291–299.
Dessai, A.G., Bertrand, H., 1995. The "Panvel Flexure" along the Western Indian continental margin: an extensional fault structure related to Deccan magmatism. Tectonophysics 241, 165–178.
Dessai, A.G., Vaselli, O., 1999. Petrology and geochemistry of xenoliths in lamprophyres from the Deccan Traps: implications for the nature of the deep crust boundary in western India. Mineralogical Magazine 63, 703–722.
Dessai, A.G., Viegas, A.A.A.A., 1995. Multigeneration mafic dyke swarm related to Deccan magmatism, south of Bombay: Implications on the evolution of the western continental margin, in: Devaraju, T. C., (Ed.). Dyke Swarms of Peninsular India. Memoir Geological Society of India 33, 435–451.
Dessai, A.G., et al., 1990. Mineralogy and petrology of some xenolith bearing alkaline dykes associated with Deccan magmatism, south of Bombay, India. European Mineralogist 2, 667–685.
Dessai, A.G., Knight, K., Vaselli, O., 1999. Thermal structure of the lithosphere beneath the Deccan Traps along the western Indian continental margin: evidence from xenoliths data. Journal of the Geological Society of India 54, 585–598.
Dessai, A.G., et al., 2004. Granulite and Pyroxenite Xenoliths from the Deccan Trap: Insight into the Nature and Composition of the lower Lithosphere beneath cratonic India. Lithos 78, 263–290.
Dessai, A.G., et al., 2009. Structure of the Deep Crust beneath the Central Indian Tectonic Zone: an Integration of Geophysical and Xenolith Data. Gondw. Res. 17, 162–170.
Devey, C.W., Stephens, W.E., 1991. Tholeiitic dykes in the Seychelles and the original spatial extent of Deccan. Journal of the Geological Society of London 148, 979–983.
Devey, C.W., Stephens, W.E., 1992. Deccan related magmatism west of Seychelles-India rift. In: Alabaster, B. C. and Pankhurst, R. J., (Eds.), Magmatism and the Causes of Continental Break-up. Geol. Soc. Spec. Pub. 68, 271–291.
Drury, M.R., van Roermund, H.L.M., 1989. Fluid assisted recrystallization in upper mantle peridotite xenoliths from kimberlites. J. Petrol. 30, 133–152.
Eggler, D.H., Furlong, K.P., 1991. Destruction of subcratonic mantle keel: the Wyoming province. In: 5th Kimberlite Conference Extended Abstract.
Evans, R.L., et al., 2011. Electrical lithosphere beneath the Kaapvaal craton, southern Africa. J. Geophys. Res. 116, B04105. doi:10.1029/2010JB007883.
Fisk, M.R., Upton, B.G., Ford, C.E., 1988. Geochemical and experimental study of the genesis of magmas of Reunion island, Indian Ocean. J. Geophys. Res. 93, 4933–4950.
Foley, S.F., 2008. Rejuvenation and erosion of the cratonic lithosphere. Nat. Geosci. 1, 503–510.
Frey, F.A., Prinz, M., 1978. Ultramafic inclusions from San Carlos, Arizona: petrologic and geochemical data bearing on their petrogenesis. Earth Planet. Sci. Lett. 38, 129–176.
Friend, C.R.L., Nutman, A.P., 1992. Response to U-Pb isotope and whole rock geochemistry to CO2 induced granulite facies metamorphism, Kabbaldurga, Karnataka, South India. Contrib. Mineral. Petrol. 111, 299–310.
Ganguly, J., Battacharya, P.K., 1987. Xenoliths in Proterozoic kimberlites from southern India : petrology and geophysical implications. In: Nixon, P.H. (Ed.), Mantle Xenoliths. John Wiley, pp. 249–265.
Gaul, O.F., et al., 2000. Mapping olivine composition in the lithospheric mantle. Earth Planet. Sci. Lett. 182, 223–235.
Geoffroy, L., et al., 1998. The coastal flexture of Disko (West Greenland), on shore expression of 'oblique reflectors'. Journal of the Geological Society of London 155, 463–473.
Geological Survey of India, 1993. Geological Map of India, Scale 1:500,000. Calcutta, India.
Glennie, E.A., 1951. Density or geological correction to gravity anomalies for the Deccan Traps, India. Montrial National Royal Austronomy and Geophysics Supplement 6, 179.
Gokarn, S.G., 2003. Electrical conductivity patterns along transects over the Indian lithospheric domains of differing temporal evolution: a review. In: Mahadevan, T.M., Arora, B.R., Gupta, K.R. (Eds.), Indian Continental Lithosphere, 53. Geological Society of India Memoir, pp. 129–147.
Gokarn, S.G., Rao, C.K., Nayak, P.N., 1992. Magnetotelluric studies across the Kurduwadi gravity feature. Physics of Earth and Planetary Interior 72, 58–67.
Gokarn, S.G., Gupta, G., Rao, C.K., 2004. Geoelectric structure of the Dharwar craton from magnetotelluric studies: Archaean suture identified along the Chitradurga-Gadag schist belt. Geophysics Journal International 158, 712–728.
Green, D.H., Hibberson, W., 1970. The instability of plagioclase in peridotite at high pressure. Lithos 3, 209–221.
Griffin, W.L., Carlswell, D.A., Nixon, P.H., 1979. Lower crustal granulites from Lesotho, South Africa. In: Boyd, F.R., Meyer, H.O.A. (Eds.), The mantle sample: inclusions in kimberlites and other volcanics. In: Proceedings of the 2nd Inter. Kimberlite Conf. 2. Amer. Geophys. Union, Washington, D.C. pp. 59–86.
Griffin, W.L., Wass, S.Y., Hollis, J.D., 1984. Ultramafic xenoliths from Bullenmerri and Gnotuk Maars, Victoria, Australia: petrology of a subcontinental crust–mantle transition. Journal of Petrolology 25, 53–87.
Griffin, W.L., O'Reilly, S.Y., Ryan, C.G., 1992. Composition and thermal structure of the lithosphere beneath South Africa, Siberia and China : proton microprobe studies. International Symposium on Cenozoic Volcanic rocks and deep-seated xenoliths of China and its Environs, Beijing, Vol. 20.
Griffin, W.L., et al., 1998. Phanerozoic evolution of the lithosphere beneath the Sino-Korean craton. In: Flower, F.M.J., Chung, S.L., Lo, C.H., Lee, T.Y. (Eds.), Mantle Dynamics and Plate Interactions in East Asia. AGU Geodynam. Ser, 27. pp. 107–126.
Griffin, W.L., et al., 1999. The Siberian lithosphere traverse: mantle terrains and the anomaly of Siberian cratons. Tectonophysics 310, 1–35.
Griffin, W.L., et al., 2003. The evolution of lithospheric mantle beneath Kalahari craton and its margins. Lithos 71, 215–241.
Griffin, W.L., et al., 2009. A translithospheric suture in the vanished 1-Ga lithospheric root of South India: evidence from contrasting lithosphere sections in the Dharwar craton. Lithos 112, 1109–1119.
Gupta, M.L., 1982. Heat flow in the Indian peninsula-its geological and geophysical implications. Tectonophysics 8, 71–90.
Gupta, M.L., Gaur, V.K., 1984. Surface heat flow and probable evolution of Deccan volcanism. Tectonophysics 105, 309–318.
Gupta, M.L., Sharma, S.R., Sundar, A., 1991. Heat flow and heat generation in the Archaean Dharwar cratons and implications for the southern Indian shield geotherm and lithospheric thickness. Tectonophysics 194, 107–122.
Gupta, S., et al., 2003. The nature of the crust in southern India: Implications for Precambrian crustal evolution. Geophys. Res. Lett. 30 (8), 1419. doi:10.1029/2002GL016770.
Hall, H.C., et al., 2007. Paleomagnetism and U–Pb geochronology of easterly trending dykes in the Dharwar craton, India: feldspar clouding, radiating dyke swarms and the position of India at 2.37 Ga. Precambrian Res.. doi:10.1016/j.precamres.2007.01.007.
Hofmann, C., Feraud, G., Courtillot, V., 2000. 39Ar/ 40Ar dating of mineral separates and whole rocks from Western Ghats lava pile: further constraints on duration and age of the Deccan Traps. Earth Planet. Sci. Lett. 180, 13–27.
Iyer, H.M., et al., 1989. High velocity anomaly beneath the Deccan volcanic province: evidence from seismic tomopgraphy. In: Proceedings of the Indian Acadamy of Sciences, (Earth and Planetary Science), 98. pp. 31–60.
Jaupart, C., Mareschal, J.C., 1999. The thermal structure and thickness of continental roots. Lithos 48, 93–114.
Jayananda, M., Peucat, J.-J., 1996. Geochronological framework of southern India. Gondwana Research Group Memoir 3, 53–75.
Jayananda, M., et al., 2006. 2.61 Ga potassic granites and crustal reworking in the western Dharwar craton, southern India: geochronologic and tectonic constraints. Precambrian Res. 150, 1–26.
Jayananda, M., et al., 2008. 3.35 Ga komatiite volcanism in the western Dharwar craton, southern India: constraints from Nd isotopes and whole-rock geochemistry. Precambrian Res. 162, 1160–1179.
Kaila, K.L., 1988. Mapping the thickness of Deccan Trap flows in India from DSS studies and inferences about a hidden Mesozoic basin in the Narmada–Tapti region. In: Subbarao, K.V. (Ed.), Deccan Flood Basalts. Geological Society of India Memoir 10, 91–116.

Kaila, K.L., et al., 1979. Crustal structure along Kavali-Udupi profile in the Indian Peninsular shield from deep seismic soundings. Journal of the Geological Society of India 20, 307–333.
Kaila, K.L., et al., 1981. Crustal structure from deep seismic sounding along Koyna II (Kelsi-Loni) profile in the Deccan Trap, India. Tectonophysics 73, 365–384.
Karmalkar, N.R., Duraiswami, R.A., 2010. Ultramafic xenoliths from Kutch, Northwest India: Samples of relict cratonic keel? In: Karmalkar, N.R., Duraiswami, R.A., Pawar, N.J., Sivaji, Ch. (Eds.), Origin and Evolution of the Deep Continental Crust. Narosa Publishing House Pvt. Ltd, India, pp. 237–260.
Karmalkar, N.R., Griffin, W.L., O'Reilly, S.Y., 2000. Ultramafic xenoliths from Kutch (NW India): Plume related mantle samples? International Geology Reviews 42, 416–444.
Karmalkar, N.R., et al., 2005. Alkaline magmatism from Kutch, NW India: Implications for plume-lithosphere interaction. Lithos 81, 101–119.
Kennedy, C.S., Kennedy, G.C., 1976. The equilibrium boundary between graphite and diamond. J. Geophys. Res. 81, 2467–2470.
Kerr, A.C., 1994. Lithospheric thinning during the evolution of large Igneous Provinces: a case study from the North Atlantic Tertiary Province. Geology 22, 1027–1030.
Kiselev, S., et al., 2008. Lithosphere of the Dharwar craton by joint inversion of P and S receiver functions. Geophys. J. Int. 173, 1106–1118.
Kobussen, A.F., Griffin, W.L., O'Reilly, S.Y., 2009. Cretaceous thermo-chemical modification of the Kaapvaal cratonic lithosphere, South Africa. Lithos 112, 886–895.
Kosarev, G.L., et al., 2013a. Heterogeneous lithosphere and the underlying mantle of the Indian lithosphere. Tectonophysics 282, 175–186. doi:10.1016/j.tecto.2013.02.023.
Kosarev, G.L., et al., 2013b. Heterogeneous lithosphere and the underlying mantle of the Indian lithosphere. Tectonophysics 282, 175–186. doi:10.1016/j.tecto.2013.02.023.
Krogstad, E.J., Hanson, G.N., Rajamani, V., 1991. U-Pb ages of zircon and sphene for two gneiss terrains adjascent to the Kolar schist belt South India: evidence for separate crustal histories. J. Geol. 99, 801–816.
Kumar, Anil, Heaman, L.A., Manikyamba, C., 2007a. Mesoproterozoic kimberlites in southern India: a possible link to 1.1 Ga global magmatism. Precambrian Res. 15, 192–204.
Kumar, P., et al., 2007b. The rapid drift of the Indian tectonic plate. Nature 449, 894–897.
Kumar, N., et al., 2013. Lithospheric structure of the southern Indian shield and adjoining oceans: integrated modelling of topography, gravity, geoid and heat flow data. Geophysics Journal International 194, 30–44.
Lee, C.T., Rudnick, R.L., 1999. Compositionally stratified cratonic lithosphere: petrology and geochemistry of peridotite xenoliths from Labait volcano tuff cone, Tanzania. In: Guney, J.J., Richarson, S.R. (Eds.), Proc. 7th Int. Kimberlite Conference, Red Roof Design, Cape Town. pp. 503–521.
Leelanandam, C., et al., 2006. Proterozoic mountain building in peninsular India: Analysis based primarily on alkaline rock distribution. Geol. Mag. 143, 195–212.
Liang, Y., Sun, C., Yao, L., 2013. A REE-in-two-pyroxene thermometer for mafic and ultramafic rocks. Geochimica Cosmochica Acta 102, 246–260.
MacKenzie, D., Sclater, J.G., 1971. Evolution of the Indian ocean since the late cretaceous. Geophysics Journal International 24, 437–528.
Mahadevan, T.M., 1994. Deep Continental Structure of India: a Review. Geological Society of India Memoir 28, 569.
Mandal, B., et al., 2018. Deep crustal seismic reflection images from the Dharwar craton, South India-evidence for Neoarchaean subduction. In: Geophysics Journal International, 212, 777–794. Indian continent, Beneath. doi:10.1002/2016JB012948.
Manglik, A., Mandal, P., 2016. Workshop on geodynamics of the Singhbhum craton: present status and future directions, CSIR-NGRI, Hyderabad. Curr. Sci. 110, 1144–1145.
Maurya, S., et al., 2016. Imaging the lithospheric structure beneath the Indian continent. J. Geophys. Res.. doi:10.1002/2016JB012948.
McDonough, W.F., Sun, S.S., 1995. The composition of the Earth. Chem. Geol. 120, 223–253.
Meert, J.G., et al., 2010. Precambrian crustal evolution of Peninsular India: a 3.0 billion year odyssey. J. Asian Earth Sci. 39, 483–515.
Menzies, M.A., Weiming, F., Zhang, M., 1993. Palaeozoic and Cenozoic lithoprobes and the loss of N120 km of Archaean lithosphere, Sino-Korean craton, China. Geological Society of London Special Publication 76, 71–81.
Menzies, M., et al., 2007. Integration of geology, geophysics and geochemistry: a key to understanding North China craton. Lithos 96, 1–21.
Mercier, J.C.C., Nicolas, A., 1975. Textures and fabrics of upper mantle peridotites as illustrated by xenoliths in basalts. J. Petrol. 16, 454–487.
Zheng, J., et al., 2006. A refractory mantle protolith in younger continental crust, east-Central China: Age and composition of zircon in the Sulu UHP peridotite. Geology 34, 705–708.
Mercier, J.C.C., Benoit, V., and Girardeau, J., (1984). Equilibrium state of diopside-bearing harzburgites from ophiolites: Geobarometric and geodynamic implications: Contributions to Mineralogy and Petrology, 85, 391–403. doi: 10.1007 /BF01150295.
Mitra, S., et al., 2006. Shear wave structure of south Indian lithosphere from Raleigh wave phase velocity measurements. Bull. Seismol. Soc. Am.. doi:10.1785/0120050116.
Morimoto, M., et al., 1988. Nomenclature of pyroxenes. Mineralogical Magazine 52, 535–550.
Mukherjee, A.B., Biswas, S., 1988. Mantle-derived spinel lherzolite xenoliths from the Deccan Volcanic Province (India): Implications for the thermal structure of the lithosphere underlying the Deccan Traps. J. Volcanol. Geotherm. Res. 35, 269–276.
Naqvi, S.M., Rogers, J.J.W., 1987. Precambrian Geology of India. Oxford Monograph on Geology and Geophysics. Clarendon Press/Oxford University Press, p. 216.
Nataf, H.C., Nakanishi, I., Andeson, D.L., 1984. Anisotropy and shear wave velocity heterogeneities in the upper mantle. Geophysics Research Letters 11, 109–112.
Negi, J.G., Pandey, O.P., Agarwal, P.K., 1986. Supermobility of hot Indian lithosphere. Tectonophysics 131, 147–156.
Negi, J.G., Agrawal, P.K., Pandey, C.P., 1987. Large variation in Curie depth and lithospheric thickness beneath the Indian subcontinent and case for magnetothermometry. Geophysics Journal of the Royal Astronomical Society 88, 763–775.
Nehru, C.E., Reddy, A.K., 1989. Ultramafic xenoliths from Wajrakarur kimberlite, India. In: Ross (Ed.), et al., Kimberlites and Related Rocks, Geological Society of Australia Special Publication, 14. pp. 745–759.
Nielsen, T.F.D., Brooks, C.K., 1981. The East Greenland rifted continental margin; an examination of the coastal flexure. Journal of Geological Society of London 138, 559–568.
Nixon, P.H., et al., 1981. Depleted and fertile mantle xenoliths from southern African kimberlites. Annual Review of Earth Planetary Sciences 9, 285–309.
Norton, I.O., Sclater, J.G., 1979. A model for the evolution of the Indian ocean and the break-up of the Gondwana. J. Geophys. Res. 84, 6803–6830.
Nutman, A.P., et al., 1992. SHRIMP U–Pb ages of detrital zircon inSargursupracrustal rocks in western Karnataka, southern India. Journal of the Geological Society of India 39, 367–374.
O'Neil, H.S.C., 1981. The transition between spinel lherzolite and garnet lherzolite and its use a geothermometer. Contrib. Mineral. Petrol. 77, 185–194.
O'Reilly, S.Y., Griffin, W.L., 1985a. A xenoliths derived geotherm for southeastern Australia and its geophysical implications. Tectonophysics 111, 41–63.
O'Reilly, S.Y., Griffin, W.L., 1985b. A xenoliths derived geotherm for southeastern Australia and its geophysical implications. Tectonophysics 111, 41–63.
Oreshin, S.I., et al., 2011. Deep seismic structure of the Indian shield western Himalaya, Ladakh and Tibet. Earth Planet. Sci. Lett. 307, 415–419.
Patro, P.K., Sarma, S.V.S., 2009. Lithospheric electrical imaging of the Deccan Traps covered region of western India. J. Geophys. Res. 114, B01102. doi:10.1029/2007JB005572.
Pattanaik, J., Ghosh, S., Dongre, A., 2020. Plume activity and carbonated silicate melt metasomatism in Dharwar cratonic lithosphere: evidence from peridotite xenoliths in Wajrakarur kimberlite. Lithos 376–377. doi:10.1016/j.lithos.2020.105726.
Pearson, D.G., et al., 1995. Stabilization of Archaean lithospheric mantle: a Re–Os isotope study of peridotite xenoliths from the Kaapvaal craton. Earth Planet. Sci. Lett. 134, 341–357.
Peng, Z.X., Mahoney, J.J., 1995. Drillhole lavas from the northwestern Deccan Traps and the evolution of Reunion hotspot mantle. Earth Planet. Sci. Lett. 134, 169–185.
Polet, J., Anderson, D.L., 1995. Depth extent of cratons as inferred from tomographic studies. Geology 23, 205–208.
Pollock, C.H., Chapman, D.H., 1977. On the regional variation of heat flow, geotherms and the thickness of the lithosphere. Tectonophysics 38, 279–296.
Putirka, K.D., 2008. Thermometers and barometers for volcanic systems. Reviews of Mineralogy and Geochemistry 69, 61–120.
Radhakrishna, B.P., Ramakrishnan, M., 1988. Archaean-Proterozoic boundary in India. Journal of the Geological Society of India 32, 263–278.
Rai, S.S., Vijay Kumar, T., Jagdeesh, S., 2005. Seismic evidence for significant crustal thickening beneath Jabalpur earthquake, 21st May, 1997 source region in Narmada-Son lineament, Central India. Geophys. Res. Lett. 32, L2306. doi:10.1029/2005GL023580.
Ramesh, D.S., Bianchi, M.B., Sharma, D.S., 2010. Images of possible fossil collision structures beneath the Eastern Ghats belt, India, from P and S receiver functions. Lithosphere 2, 84–92.
Ravi Kumar, M., Mohan, G., 2005. Mantle discontinuities beneath the Deccan volcanic province. Earth Planet. Sci. Lett. 237, 252–263.
Reddy, P.R., et al., 2003. Deep seismic reflection and refraction/wide angle reflection studies along Kuppam-Palani transect in southern granulite terrain in India. In: Ramakrishnan, M., (Ed.), Tectonics of Southern Granulite Terrain. Geological Society of India Memoir 50, 79–106.
Replumaz, A., et al., 2004. 4-D evolution of SE Asia's mantle from geological reconstructions and seismic tomography. Earth Planet. Sci. Lett. 221, 103–115.
Rogers, N.W., 1977. Granulite xenoliths from the Lesotho kimberlite and the lower continental crust. Nature 277, 681–684.
Roy, S., Mareschal, J.-C., 2011. Constraints on the deep thermal structure of the Dharwar craton, India, from heat flow, shear wave velocities and mantle xenoliths. J. Geophys. Res. 116, B02409. doi:10.1029/2010JB007796.
Roy, S., Rao, R.U.M., 2000. Heat flow in the Indian shield. J. Geophys. Res. 105, 25587–25604.
Rudnick, R.L., McDonough, W.F., Orpin, A., 1994. Northern Tanzanian peridotite xenoliths: a comparison with Kaapvaal peridotites and inferences on metasomatic interactions. In: Meyer, H.O.A., Leonardo, O.H. (Eds.), Proc. 5th Int. Kimberlite Conference, 1 Rio de Janeiro, Companhia de Pesquisa de Recursos Minerais. pp. 336–353.
Ryan, C.G., Griffin, W.I., Pearson, N.G., 1996. Garnet geotherm: a technique for the derivation of P-T data from Cr-pyrope garnets. J. Geophys. Res. 101, 5611–5625.
Rychert, C.A., Shearer, P.M., 2009. A global view of the lithosphere-asthenosphere boundary. Science 324, 495–498.
Sachtleben, T., Seck, H.A., 1981. Chemical control of Al-solubility in orthopyroxene and its implications on pyroxene geothermometry. Contrib. Mineral. Petrol. 78, 157–165.
Schmidberger, S.S., Francis, D., 1999. Nature of the mantle roots beneath the north American craton: Mantle xenolith evidence from Somerset Island kimberlites. Lithos Special Issue 48, 195–216.
Shalivahan, S.S., et al., 2014. Thin lithosphere-asthenosphere boundary beneath eastern Indian craton. Tectonophysics 612–613, 128–133.
Shapiro, S.S., Hager, B.H., Jordan, T.H., 1999. Stability and dynamics of the continental tectosphere. Lithos 48, 115–133.
Simonetti, A., et al., 1998. Geochemical and Nd, Pb, and Sr isotope data from Deccan alkaline complexes-inferences for mantle sources and plume-lithosphere interaction. J. Petrol. 39, 1847–1864.

Singh, A., et al., 2014. Continental scale body wave tomography of India: evidence for attrition and preservation of lithospheric roots. Geochemistry Geophysics Geosystems 15, 658–675.
Smith, A.D., 1993. The continental mantle as a source of hotspot volcanism. Terra Nova 5, 452–460.
Sodoudi, F., et al., 2013. Seismic evidence for stratification in composition and anisotropic fabric within the thick lithosphere of Kalahari craton. Geochemistry Geophysics Geosystems 14, 5393–5412. doi:10.1002/2013GC004955.
Srinivas Rao, G., et al., 2014. Lithosphere structure and upper mantle characteristics below the Bay of Bengal. Geophysics Journal International 206, 675–695.
Stewart, K., Rogers, N., 1996. Mantle plumes and lithosphere contribution to basalts from southern Ethiopia. Earth Planet. Sci. Lett. 139, 195–211.
Storey, M., et al., 1995. Timing of hot-spot related volcanism and break-up of Madagascar and India. Science 267, 852–855.
Swami Nath, J., Ramakrishnan, M., 1981. Early Precambrian supracrustals of southern Karnataka. Geological Survey of India Memoir 112, 1–350.
Takin, M., 1966. An interpretation of the positive gravity anomaly over Bombay and west coast of India. Geophysics Journal of the Royal Astronomical Society 11, 527–537.
Torskvik, T.H., et al., 2000. Late Cretaceous India-Madagascar fit and the timing of break-up related magmatism. Terra Nova 12, 220–224.
Vijaya Rao, V., et al., 2015a. Upper crust of the Archean Dharwar craton in southern India using seismic refraction tomography and its geotectonic implications. Geophysics Journal International 200, 652–663.
Vijaya Rao, V., et al., 2015b. Crustal velocity structure of the Neoarchean convergence zone between the eastern and western blocks of Dharwar Craton, India from seismic wide-angle studies. Precambrian Res. 266, 282–295.
Walter, M.J., 1998. Melting of garnet peridotite and the origin of komatiite and depleted lithosphere. J. Petrol. 39, 29–60.
Wells, P.R.A., 1977. Pyroxene thermometry in simple and complex systems. Contrib. Mineral. Petrol. 62, 129–139.
Wilshire, H.G., Shervais, J.W., 1975. Al-augite and Cr-diopside xenoliths in basaltic rocks from western United States. Physics and Chemistry of the Earth 9, 252–272.
Witt-Eickschen, G., Seck, H.A., 1987. Temperature history of sheared mantle xenoliths from west Eifel, Germany: evidence for mantle diapirism beneath the Rhenish Massif. J. Petrol. 28, 475–493.
Wood, B.J., Banno, S., 1973. Garnet-orthopyroxene and orthopyroxene-clinopyroxene relationships in simple and complex systems. Contrib. Mineral. Petrol. 42, 109–121.
Xu, X., O'Reilly, S.Y., Griffin, W.L., 1996. A xenoliths-derived geotherm and the crust mantle boundary at Qilin, southeastern China. Lithos 38, 41–62.
Xu, X., et al., 2008. Re-Os isotopes in mantle xenoliths from eastern China: age constraints and evolution of lithospheric mantle. Lithos 102, 49–64.
Zandt, G., Ammon, C.J., 1995. Continental crust composition constrained by measurement of crustal Poisson's ratio. Nature 374, 152–154.
Zheng, J., et al., 2004. U-Pb and Hf-isotope analysis of zircons in mafic xenoliths from Fuxian kimberlites: evolution of lower crust beneath North China craton. Contrib. Mineral. Petrol. 148, 79–103.